

PHORTEX: Physically-Informed Operational Robotic Trajectories for (Scientific) Expeditions

Victoria L. Preston*

Aeronautics and Astronautics

Massachusetts Institute of Technology
Cambridge, MA 01275
vpreston@csail.mit.edu

Genevieve E. Flaspoher*

Electrical Engineering and Computer Science
Massachusetts Institute of Technology
Cambridge, MA 01275
geflaspo@csail.mit.edu

Daniel Yang

Electrical Engineering and Computer Science
Massachusetts Institute of Technology
Cambridge, MA 01275
dxyang@csail.mit.edu

John Fisher III

CSAIL
Massachusetts Institute of Technology
Cambridge, MA 01275
jfisher@csail.mit.edu

Anna P. M. Michel

Applied Ocean Physics and Engineering
Woods Hole Oceanographic Institution
Woods Hole, MA 02543
amichel@whoi.edu

Nicholas Roy

CSAIL
Massachusetts Institute of Technology
Cambridge, MA 01275
nickroy@csail.mit.edu

Abstract

Robots are uniquely well-suited for *in situ* sample collection for scientific expeditions. Many target phenomena in scientific studies are *spatiotemporal distributions*, evolving across space and over timescales relevant for planning useful sampling trajectories. However, the underlying dynamics of ~~some~~^{such as} a phenomenon are typically unknown and partially observable, posing significant uncertainty for an autonomous decision-maker. Further, state-of-the-art robotic platforms used for scientific expeditions are operationally limited in the total number of deployments that can be executed in a given expedition, and their ability to act under their own agency, restricted to executing pre-set trajectories (e.g., uniform-coverage lawnmowers). Here, we propose an autonomy framework PHORTEX: **P**Hysically-informed **O**perational **R**obotic **T**rajectories for **E**Xpeditions, that enables operationally restricted robots to quickly improve their per-deployment performance for sampling complex, spatiotemporal distributions. PHORTEX uses a novel deployment-by-deployment autonomy schema that leverages a history of robotic observations to incrementally improve ~~the sampling~~^{the sampling strategy} performance of fixed sampling trajectories over an entire expedition. Within this schema, we use a novel physically-informed probabilistic model that imposes scientific knowledge as an inductive bias suitable for sample-efficient learning, and a trajectory optimizer which chains operationally-approved primitives (e.g. lawnmowers) for more expressive single-deployment missions. We formulate PHORTEX for a specific instance of spatiotemporal scientific expedition and robot: deep-sea hydrothermal plume charting with autonomous underwater vehicle (AUV) *Sentry*, and demonstrate via simulation and field trials in the Gulf of California that *Sentry* using PHORTEX collects just as many samples as the best human-designed sampling missions, and improves the spatial and temporal diversity of the sample set relevant for scientific post-expedition analyses.

1 Introduction

Transient, dynamic phenomena—deep-sea hydrothermal plumes, algal blooms, warm core eddies, lava flows—are of interest in many disciplines of observational science. *Expeditionary science* encapsulates the observational sciences that require *in situ* sample collection of environmental phenomena for scientific discovery and model development. In such cases, the environmental targets are typically impossible to observe using remote means (e.g., satellites) either due to desired spatial and temporal resolution, environment adversity (e.g., the deep sea, within closed structures), or the nature of the scientific target of interest and corresponding sensing equipment (e.g., taxonomy of algae requires physically processing water samples). Expeditionary science is, by definition, conducted in a partially-observable environment, and creating comprehensive pictures of these environments is further complicated by spatiotemporal distributions (*e.g.*, dynamic phenomena), such as moving seafloor plumes.

Mobile robots, equipped with heterogeneous sensor payloads, are increasingly used in the expeditionary sciences to perform broad surveys, typically executing preset trajectories hand-designed by human scientists (e.g., [Camilli et al., 2010]). Although in dynamic environment this open-loop execution can result in sparse measurements of the target phenomenon or can miss short-lived events entirely [Flaspoehler et al., 2019], these operations remain the state-of-the-art in practical deployments due to their relative ease to encode, limited computational capacity of the platforms, and predictability of robot actions to outside supervisors. However, given the cost of scientific field operations and the value of the data collected, it is critical to improve the efficacy of robots as scientific tools.

Enabling robots to collect scientific observations of spatiotemporal phenomena requires an autonomy stack that can integrate observations from heterogeneous science sensors into an inferred dynamical model (or belief) and use this model to plan informative trajectories for a specific scientific objective while honoring operational constraints. This kind of autonomy poses many challenges for integrating probabilistic modeling and decision-making. Previous work in informative path planning (IPP) [Hitz et al., 2017], adaptive sampling/experimental design [Krause et al., 2008a], and decision-making under uncertainty [Sunberg and Kochenderfer, 2018] has tackled aspects of the expeditionary science problem, especially in static environments using data-driven models and information-based rewards. However, existing methodologies do not trivially extend to spatiotemporal environments, leaving key challenges such as model and dynamics learning and decision-making in realistic spatiotemporal environments, unaddressed.

In this paper, we study robot autonomy for a particular class of scientific spatiotemporal phenomena, deep-sea buoyant plumes. Buoyant plumes are driven by hydrothermalism. Super-heated water enriched with chemicals rises through the cold and chemically-poor background seawater, mixing (entraining) as it rises, until reaching a point of neutral buoyancy with the ambient seawater. At the neutrally-buoyant layer, plume-derived fluid spreads out over the isopycnal that describes constant density. Metals, sediment, and other suspended particulates carried by this fluid may then be re-deposited onto the seafloor from the neutrally-buoyant layer, and persisting chemicals may be digested by microbes. Understanding the fate of chemicals and particulates in hydrothermal plumes is of significant interest to biogeochemists and physical oceanographers; however, directly studying plumes in the water column is a significant challenge due to the state uncertainty driven by unseen advective forces (e.g., deep currents, topographic updrafts), diffusive mixing, and unknown venting characteristics that dictate plume formation and the extreme partial observability of point *in situ* measurements in a continuous three-dimensional volume over time. A robot charting a hydrothermal plume must be able to forecast where and when it will intersect with different parts of the plume in order to collect useful observations.

In addition to the technical challenges of determining a sensing strategy in the face of highly uncertain and dynamic phenomena, also create planning challenges. In this paper, we also study the impact of robot operational constraints on planning efficacy. Here, we consider constraints introduced by a specific robot, autonomous underwater vehicle (AUV) Sentry. AUV Sentry, operated by Woods Hole Oceanographic Institution (WHOI) and the National Deep Submergence Facility (NDSF) [Kaiser et al., 2016], which can only execute pre-determined regular trajectories like lawnmowers or spirals, making online adaptation impossible. This limitation necessitates developing a novel deployment-by-deployment framework which iteratively improves a forecast of plume waters from an entire robot deployment with a fixed trajectory to enhance the performance of the fixed trajectory of the next deployment.

PHORTEX: PHysically-informed Operational Robotic Trajectories for EXPeditions is our unified framework for spa-

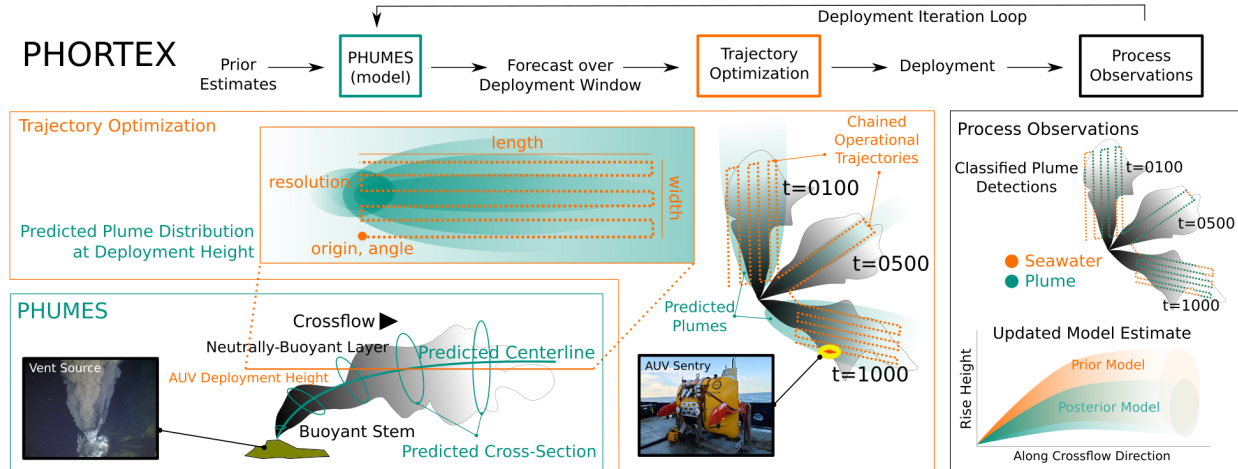


Figure 1: An overview of PHOREX: **PH**ysically-informed **O**perational **R**obotic **T**rajectories for **E**Xpeditions. Over the course of an expedition, an autonomous vehicle is deployed several times. In preparation for a deployment, PHUMES is used to generate a probabilistic forecast of the target spatiotemporal distribution. PHUMES can be seeded with prior information from scientific knowledge, data of opportunity from other deployed sensing equipment, or previous robot deployments. A trajectory optimizer is given the forecasts and modifies the parameters of a trajectory primitive. Several primitives are chained together to form a complete deployment trajectory. The robot is then deployed and executes the ~~set~~ trajectory. Following a deployment, *in situ* observations from multiple heterogeneous science sensors are collected from the robot and fused into a data product that can be used to train Update PHUMES, and the deployment planning process iterates. Here, the task of hydrothermal plume charting with AUV *Sentry* is illustrated. PHUMES generates an estimate of temporally-evolving plume centerlines and cross-sections from estimates of vent characteristics and fluid crossflow (e.g., current). For a given height that *Sentry* can operate (and is constrained to operate for any given primitive), chains of uniform coverage lawnmowers are optimized (over parameters such as length, width, resolution, origin, and global angle) with respect to the plume forecast to intersect and track the plume over the course of a deployment window. Following a *Sentry* deployment, observation locations are classified as binary plume detections from analysis of several science sensors. This product is then used to update the PHUMES model of plume centerline and cross-section over time. The new PHUMES model is then used to plan the next deployment of *Sentry*. ^{*new surveys?*}

tiotemporal distribution forecasting (independently called PHUMES: **P**Hysically-informed **U**ncertainty **M**odels for Environment Spatiotemporality) and operationally-realistic deployment-by-deployment autonomy (Fig. 1). Using *in situ* measurements, a physically-informed probabilistic model is trained to forecast the location of plume fluids over time. These forecasts are then served to a trajectory optimizer which chains parameterized primitives (e.g., lawnmowers) to strategize plume intersections over the course of multi-hour deployments. We demonstrate PHORTEX in the hydrothermal plume charting task with AUV *Sentry*, and show results from a field campaign to the Guaymas Basin in the Gulf of California from November 2021. Trajectories executed using PHORTEX collect at least as many observations as hand-designed trajectories by scientists, and significantly improve upon spatial and temporal diversity of those samples (that is, samples are collected from throughout an entire deployment rather than at a single time, and over the entire spatial extent, rather than at a single location). Further, we show that this sample diversity leads to improved inference performance over the true underlying vent characteristics of interest to scientists, including estimates of vent area, chemical flux, and temperature. In simulation, we quantify the performance of PHORTEX, particularly focusing on the properties of the forecasting procedure PHUMES and deployment-by-deployment learning inference. We conclude with a discussion of the generalization capabilities of PHORTEX and remaining open challenges in autonomy for scientific expeditions.

1.1 An Instance of Science Expeditions: Charting Deep Sea Hydrothermalism

Hydrothermal vents in the ocean were first observed in 1977 [Corliss et al., 1979] at the Galapagos Rift, and since have been a concerted focus of geodynamical and biogeochemical studies. Venting sites, energized by magmatic sources, release fluids between 20-400 °C (background deep ocean temperatures are approximately 2 °C) and imbued with minerals, metals, dissolved gases, and other compounds [Jannasch and Mottl, 1985, Martin et al., 2008]. These warm, nutrient-pumping sites in the deep ocean have created oases of unique micro- and macro-fauna [Corliss et al., 1979]. Detection and characterization of seafloor hydrothermal venting are critical for understanding fundamental interactions between the deep ocean, its underlying basaltic crust, the deep biosphere, and (bio)geochemical fluxes.

We build on a wealth of work that has primarily focused on localizing venting plume sources (e.g., Jakuba, 2007, McGill and Taylor, 2011, Nakamura et al., 2013, Paduan et al., 2018, Mason et al., 2020, Wang et al., 2020, Kim et al., 2020), leveraging ship-based acoustics, towed instrument rosettes, remotely-operated vehicles (ROVs), submersibles, and autonomous underwater vehicles (AUVs). Source discovery remains an important area of research, as hundreds of vents are hypothesized to exist and remain undiscovered in the deep ocean [Beaulieu et al., 2015]; however, we consider how science at the hundreds of vents that have been successfully identified can be advanced. Thus, we pose a complementary problem to source discovery: given a venting source, what impact do the venting fluids have on the local environment? In this complementary framing, rather than using detections of a plume as a means of source localization, the detections themselves are the valuable data product for scientific inquiry. By placing instruments throughout an evolving plume structure over multiple length- (meter to kilometer) and time- (hours to days) scales to collect dense in-plume measurements, previously intractable questions with respect to microbial lifecycle and transport, carbon cycling, and anomalous water mass formation, can be approached.

Don't include the inside parentheses, for better alignment.

The problem of charting hydrothermal plumes inherently requires grappling with uncertainty due to the extreme partial observability of point *in situ* measurements in a continuous three-dimensional volume over time influenced by complicated spatiotemporal dynamics of water mixing, tidal advection, and chaotic turbulence. This is exacerbated by the necessity of inferring future states of the plume distribution to enable planning informative trajectories for the robot. Charting hydrothermal plumes requires solving both an *inverse problem* of extracting the dynamical representation from *in situ* observations, and a *forward problem* of simulating those dynamics into future states. In PHORTEX, we explicitly tackle both of these problems in our belief representation framework PHUMES, which blends a numerical hydrothermal plume model with Bayesian probabilistic representations that can be used to optimize AUV sampling trajectories for plume charting.

1.2 Closing the Loop: Expedition Logistics for Deep Sea Robotics

Oceanographic research expeditions require chartering a research vessel that can house scientific teams for weeks at a time, provide workspaces for these scientific and engineering parties, store scientific equipment, facilitate deployment and recovery of scientific instruments, withstand variable sea-states, and transit many thousands of kilometers for any given expedition. Undertaking an oceanographic expedition typically requires coordination and collaboration between different scientific stakeholders, captain and crew aboard a vessel, and external teams that maintain and operate the scientific equipment.

Robotic platforms that are deep sea capable (“deep sea” in this work refers to any depths below the mesopelagic zone starting at 1000 m) are assets that are requested on a per-expedition basis. A specialized team is typically deployed with the vehicle, responsible for vehicle maintenance and working with the scientific leader to design and execute missions while at sea. Assets like AUV *Sentry* may be deployed on tens of expeditions each year and operated approximately two-thirds of the year in total. To minimize risk of vehicle loss or damage, AUVs like *Sentry* are flown in fixed survey patterns that can be easily verified before a dive and monitored while underway. Indeed, rudimentary adaptive behaviors are not inherently possible on many AUVs, in part due to this risk aversion and in part due to logistical hurdles such as the lack of onboard computing infrastructure and limited communication bandwidth between ship computers and the robot due to attenuated acoustic modem throughput.

Under the constraint of pre-determined trajectory execution for each robotic deployment, the typical workflow for

using AUVs by the science party is to provide a set of coordinates and desired trajectory survey resolution to vehicle engineers, which then translate these parameters into a safe multi-hour survey. The robot is then deployed for a single “dive” in which it executes this survey. At the conclusion of the dive, hours later, data products are available for review by the science team, and a new plan is generated during vehicle cycling time (on the order of a few hours).

Data products from a single dive may contain hundreds of thousands of point measurements from multiple heterogeneous sensors. For hydrothermal plume monitoring, a combination of these sensor streams need to be used to make confident plume detections [Jakuba, 2007], but information about exact tidal state, state of the venting source, and background sea characteristics are not available in these products, and can require fusing data products from other instruments deployed on a cruise, if available at all. The complexity of the data products makes performing “closed loop” science, in which these products directly inform a new mission, operationally challenging at sea. This is particularly true when the design of a new mission requires not just deep analysis of collected data, but forecasting the implications of those observations onto a new day, new site, or new scientific objective.

Our work aims to alleviate the burden of “closing the loop” onboard a research vessel for AUV operations. Situated as a data ingestor, model, forecaster, and planner between AUV dives, PHORTEX generates trajectories that respect operational constraints of the AUV, incorporates science tasks, ^{I understand what's going on, but up front} intuition, and priors directly into a model, fuses opportunistic data from other instruments/platforms, and provides aggregated data products and physically-meaningful estimates for scientific verification. Our autonomy stack and operational suggestions enables both algorithmic and human decision-makers at sea to maximize deployment-by-deployment utility of AUV missions.

1.3 Contributions

In this article, we present:

- PHORTEX: **P**hysically-informed **O**perational **R**obotic **T**rajectories for **E**Xpeditions, an autonomy stack designed to enable informative sample collection of a spatiotemporal distribution under realistic robotic operational constraints for scientific expeditions,
- a *deployment-by-deployment* formulation of PHORTEX which iteratively improves robot performance across an entire expedition by leveraging collective past experience,
- PHUMES: **P**hysically-informed **U**ncertainty **M**odels for **E**nvironment **S**patiotemporality, a novel model within PHORTEX which leverages domain scientific knowledge of a target phenomenon within a probabilistic framework to compute practical-time, sample efficient dynamics forecasts that are suitable for informative trajectory optimization,
- a trajectory optimizer which chains together operationally-approved trajectory primitives (e.g., lawnmowers),
- a specific formulation of PHORTEX and its constituent components for the problem of deep sea hydrothermal plume mapping, with constraints provided by the state-of-the-art oceanographic AUV *Sentry*,
- a specialized data fusion scheme for plume detection classification for the purposes of updating PHUMES from real *in situ* scientific observations,
- and a demonstration of PHORTEX in simulation and a significant field trial at the Gulf of California in the Guaymas Basin.

2 Problem Formulation

During scientific expeditions, the objective of a robot is to collect informative measurements as defined by a task-specific query (e.g., reduce uncertainty over a quantity, find the global optimum in a distribution, track a moving target). In the instance of hydrothermal plume charting, the goal is to map ~~chart~~ the spatiotemporal structure of a buoyant

I really think a particular sentence at the bottom
is. Let's discuss this
Schorr.

plume using a dynamically constrained AUV. Such a chart enables scientists to infer relevant scientific properties of generating vents (e.g., chemical flux) and to ~~chart~~ advance detailed models of deep-sea interactions and nutrient cycling.

2.1 Scientific Expeditions as a Sequential Decision-Making Problem

These missions require a robot to make a sequence of decisions to collect scientifically useful measurements of an unknown, partially-observable spatiotemporal environment under operational constraints. We formulate this sequential decision-making problem as a partially observable Markov decision-process (POMDP). Let $\Pi(\cdot)$ denote the space of probability distributions over the argument. A finite horizon POMDP can be represented as tuple: $(\mathcal{S}, \mathcal{A}, T, R, O, b_0, H, \gamma)$, where \mathcal{S} are the states, \mathcal{A} are the actions, and \mathcal{Z} are the observations. At planning iteration t , the agent selects an action $a \in \mathcal{A}$ and the transition function $T : \mathcal{S} \times \mathcal{A} \rightarrow \Pi(\mathcal{S})$ defines the probability of transitioning between states in the world, given the current state s and control action a . The transition function governs both how the state of the robot will evolve, given a chosen action, and the potentially stochastic evolution of the underlying spatiotemporal environment. After the state transition, the agent receives an observation according to the observation function $O : \mathcal{S} \times \mathcal{A} \rightarrow \Pi(\mathcal{Z})$, which defines the probability of receiving an observation, given the current state s and previous control action a . The reward function $R : \mathcal{S} \times \mathcal{A} \rightarrow \mathbb{R}$ serves as a specification of the task, assigning the states of the world that are useful for a given scientific objective high reward and others low reward. A POMDP is initialized with belief $b_0 \in \Pi(\mathcal{S})$ — an initial probability distribution over state — and plans over horizon $H \in \mathbb{Z}^+$ with discount factor $\gamma \in [0, 1]$.

As the robot moves through the world, it selects actions and receives observations. Since the state of the world is not directly observable in a POMDP, the robot maintains a probability distribution over possible states (i.e., belief) and must update this distribution each time it takes an action and receives an observation. Given the transition and observation models, the belief can be updated directly using ~~Bayes rule~~ using a Bayes filter [Särkkä, 2013]:

$$\tau(b_{t-1}, a_{t-1}, z_t) = b_t \triangleq \Pi(S_t | a_0, z_0, \dots, a_{t-1}, z_{t-1}, z_t) \quad (1)$$

$$= \Pi(S_t | b_{t-1}, a_{t-1}, z_t) \quad (2)$$

$$= \frac{\int_{s \in \mathcal{S}} O(s, a_{t-1}, z_t) T(s, a_{t-1}, s') b_{t-1}(s')}{\Pi(z_t | b_{t-1}, a_{t-1})} \quad (3)$$

where $\tau(b, a, z)$ is the updated belief after taking control action a and receiving observation z (Eq. 3). Unfortunately, Eq. (3) is intractable to compute directly and an approximate Bayesian inference procedure is required to represent the belief (e.g., Kalman filter [Welch et al., 1995], particle filter [Silver and Veness, 2010], or variational methods).

Due to the stochastic, partially observable nature of current and future states, the realized reward in a POMDP is a random variable. Optimal planning is defined as finding a horizon-dependent policy $\{\pi_t^* : \Pi(\mathcal{S}) \rightarrow \mathcal{A}\}_{t=0}^{H-1}$ that maximizes expected reward: $\mathbb{E} \left[\sum_{t=0}^{H-1} \gamma^t R(S_t, \pi_t(b_t)) \mid b_0 \right]$, where b_t is the updated belief at time t , conditioned on the history of actions and observations. The recursively defined horizon- h optimal value function V_h^* quantifies, for any belief b , the expected cumulative reward of following an optimal policy over the remaining planning iterations: $V_0^*(b) = \max_{a \in \mathcal{A}} \mathbb{E}_{s \sim b}[R(s, a)]$ and

$$V_h^*(b) = \max_{a \in \mathcal{A}} \mathbb{E}_{s \sim b}[R(s, a)] + \gamma \int_{z \in \mathcal{Z}} \Pi(z | b, a) V_{h-1}^*(\tau(b, a, z)) dz \quad h \in [1, H-1], \quad (4)$$

The optimal policy at horizon h is to act greedily according to a one-step look ahead of the horizon- h value function. However, Eq. (4) is intractable for large or continuous state, action, or observation spaces and thus the optimal policy must be approximated. Much of the art of practical decision-making uncertainty is making well-designed algorithmic and heuristic choices that enable efficient and robust planning algorithms.

2.2 Sequential Decision-Making with AUV *Sentry*

AUV *Sentry* is capable of autonomously navigating between given waypoints using a closed-loop controller and state estimator that uses acoustic ranging between the robot and the ship to set latitude, longitude, and depth coordinates. At present, *Sentry* is not capable of *underway* decision-making in which waypoints are adaptively set on-the-fly while the robot is executing its mission. The lack of underway abilities is both a logistical and intentional hurtle. Logistically, there are not appropriate computational resources available in the robot itself, and due to the reliance of acoustic communication between the robot and ship, data from *Sentry* cannot be streamed to an external computing resource densely enough to be informative (science data communication between ship and robot is 0.02 Hz assuming no packet loss, and only a subset of sensor data can be made available in any given packet). Intentionally, *Sentry* trajectories are rigorously vetted before each dive using bathymetric maps of the target region and dynamics validation schemes. Extreme (and warranted) risk aversion to losing or damaging *Sentry* makes underway plan changes not part of normal operating procedures.

Thus, to enable sequential decision-making with *Sentry* requires consideration of *deployment-by-deployment* autonomy. Unlike underway decision-making, deployment-by-deployment autonomy does not modify the AUV trajectory in real-time, but instead leverages the “down-time” between robot deployments to post-process data, update a belief model about the environment, and plan a new fixed trajectory for the next deployment to execute. This honors the strong requirement that each deployment must pass through a rigorous safety and validation check, while enabling adaptive search behavior based on accrued knowledge. Thus, each planning “step” or iteration in the POMDP framework is an entire deployment of *Sentry*. In the following section, the implications of this constraint are codified within a POMDP framework.

2.3 Charting Hydrothermalism as a POMDP

The state space \mathcal{S} The state space of the plume-charting POMDP consists of the joint continuous states of the environment (i.e., the plume) and the robot. The environment state will be represented by a d -dimensional vector of continuous plume parameters $\mathbf{x}_p \in \mathbb{R}^d$ and a current vector $\mathbf{x}_c \in \mathbb{R}^2$ that contains the heading and velocity of the prevailing crossflow, which vary in time and drive the movement of the plume. The robot state will be represented by a vector $\mathbf{x}_r \in \mathbb{R}^3$ that represents the latitude, longitude, and depth of the robot.

The action space \mathcal{A} The action space of the plume-charting POMDP consists of sequences of parameterized lawn-mower trajectory primitives. The selection of the “lawnmower” as the base primitive was given by *Sentry* operators. By chaining lawnmower trajectories together during a deployment, a relatively expressive action set is available. Each trajectory primitive is parameterized by a set of real-valued parameters $\theta \in \Theta \subseteq \mathbb{R}^b$, including notions of scale, resolution, and global position in the environment. The robot’s action set then consists of sequences of parameterized trajectories, i.e., $\mathcal{A} = \Theta^n$, $n \in \mathbb{Z}^+$. The number of trajectory objects and the altitude or depth for which a trajectory will be executed for a given chain is fixed *a priori* to planning. Notably, by choosing lawnmowers as the core trajectory primitive, we are implicitly enforcing exploration behavior during a deployment, even if optimizing over an exploitative reward function.

The transition function T The transition function $T(s, a, s')$ will be decomposed into a plume transition T_p , a current transition T_c , and a robot transition function T_r .

- The plume state parameters \mathbf{x}_p , e.g., venting characteristics like plume exit velocity or vent temperature, are assumed to be constant and therefore the plume transition function T_p is given by: $T_p(\mathbf{x}_p, a, \mathbf{x}'_p) = \delta_{\mathbf{x}_p=\mathbf{x}'_p} \forall a \in \mathcal{A}, \mathbf{x}_p, \mathbf{x}'_p \in \mathbb{R}^d$. Although it is possible for plume parameters to vary on a timescale relevant to a robotic deployment (over the course of hours [Chevaldonné et al., 1991]), the overall impact to gross features of plume rise height, bend angle, and cross-sectional area is essentially negligible.
- The current transition function T_c is more complex and driven by tidal cycles, local bathymetry, and deep sea currents. We will learn the current transition function $T_c(\mathbf{x}_c, a, \mathbf{x}'_c) = \delta_{\mathbf{x}'_c=h(\mathbf{x}_c)} \forall a \in \mathcal{A}, \mathbf{x}_c, \mathbf{x}'_c \in \mathbb{R}^2$.

I am not fully sure if this is right.
So far, some is right.
But the details don't fit.
You still deserve a grade?

Write down what you said that
you didn't write here.
Too abstract, need to
connect it with things actually
occur.

This idea needs more
explanation earlier.

Same as previous comment.

from point observations of current magnitude and heading from an ~~external~~^{second ins system} sensor (described in detail in Section 4.2). The use of an ~~external~~ makes learning this transition function independent of robot actions. However, if a similar sensor were available on the robot, this learned transition function would be dependent on robot actions.

a sensor that is not part of the robot "external" could mean on the outside of the robot's hull.

- The robot transition function T_r assumes that the robot's waypoint controller is deterministically able to execute a planned trajectory: $T_r(\mathbf{x}_r, a, \mathbf{x}'_r) = \delta_{\mathbf{x}'_r=g(\mathbf{x}_r, a)}$, where the function g evaluates the goal waypoint of the trajectory given by a . Although there is some uncertainty in the robots transition, in practice in our field application, localization and control were well-solved problems and pose uncertainty contributed minimally to the robot's task execution compared with uncertainty about the plume state.

The reward function R The reward function for the plume-charting POMDP encodes the robot's objective to produce a comprehensive map of the plume. We choose to approximate this objective by rewarding the robot for collecting observations of “plume fluids”, i.e., water that is expected to be derived from hydrothermal vents as indicated by our belief of the environmental state $R([\mathbf{x}_p, \mathbf{x}_c, \mathbf{x}_r]^\top, a) = \mathbb{I}[\text{in_plume}(\mathbf{x}_p, \mathbf{x}_c, \mathbf{x}_r, a)]$. Coupled with the constraint of using lawnmower trajectories, this relatively simple heuristic reward achieves a useful balance of explore-exploit characteristics without the need for computing a comparatively expensive information theoretic reward.

The observation space \mathcal{Z} The robot carries a variety of scientific sensors. We propose a sensor model that fuses and converts these complex, continuous scientific observations into a single binary measurement that classifies a particular observation instance as “in-plume” or “out-of-plume” (see Section 4.1). Separately, observations of crossflow magnitude and heading are available. Therefore, the observation space of the robot is the set of vector-valued binary observations of plume occupancy and continuous observations of crossflow magnitude and heading, respectively: $\mathcal{Z} = [\{0, 1\}, \{\mathbb{R}^+\}, \{(-180, 180)\}]^n n \in \mathbb{Z}^+$.

Robot might object to this
reward. I'm doing my part.
We need to either 1) say nothing
or 2) acknowledge
the negative or 3) acknowledge
it might not be the right thing to
do at this time.

This paragraph is somewhat
too specific and not specific
enough.

The measurement function O The measurement function encodes the complex relationship between the plume parameters, prevailing current, and robot state with the heterogeneous scientific sensors on the robot, each with their own complex sensor physics. Our measurement function consists of two pieces: 1) an analytical plume model that maps plume parameters \mathbf{x}_p and crossflow state \mathbf{x}_c to the distribution of plume fluids in a 3D volume over time (see Section 4.3), and 2) a binary pseudo-sensor that fuses signals from the heterogeneous sensing payload into binary plume detections that can be directly compared to the output of the analytical plume model.

Well, Euler's paragraph is
more appropriate than ours.
It's probably better to just copy
it out of the paper.

The horizon H and discount factor γ In deployment-by-deployment autonomy, the horizon H can be set to be equal to the total number of deployments to be conducted during an expedition and the discount factor γ set to 1.0. However, practically the state of *Sentry* at the end of one deployment has little or no impact on its achievable reward in the subsequent deployment due to the delayed nature of deployments and the requirement that *Sentry* always start and end on a stationary ship. This has the impact of setting $\gamma = 0$ and breaks the finite-horizon sequential decision making problem into a sequence of horizon-1 planning problems. This reduces the capacity of the planner to reason about long-term, multi-dive information gathering actions, but computationally simplifies the planning problem.

3 Background and Related Work

Don't put this after problem formulation.
Either put it before formulation or at the
end of the paper.

3.1 Informative Path Planning

Informative path planning (IPP) is a broad technical field which develops adaptive sampling frameworks for mobile platforms which optimizes trajectories over informative metrics. Several common information measures in environmental sensing applications include:

Unjustified. Needs explanation.

- Upper-Confidence Bound (UCB) [Agrawal, 1995, Auer, 2002, Snoek et al., 2012] of the form $R_{UCB} = \mu(\mathbf{x}) + \sqrt{\beta\sigma(\mathbf{x})}$ which is the sum of predictive mean μ and variance σ at queries \mathbf{x} . UCB is submodular [Nemhauser

What do we know
list. Max it =
Q & P

et al., 1978].

- Probability of Improvement (PI) [Snoek et al., 2012, Kushner, 1964]; a probability measure of whether a query x will be better than the current best measurement x^* .
- Expected Improvement (EI) [Snoek et al., 2012, Jones et al., 1998]; a measure of how much better a proposed query x will be compared to the current best measurement x^* .
- Predictive Entropy Search (PES) [Hennig and Schuler, 2012, Hernández-Lobato et al., 2014]; a measure of the conditional entropy between a query x and a predicted optimizer of a distribution $f(\cdot)$, x^* .

IPP decision-making frameworks can be offline or online. Canonical offline IPP techniques for pure information-gathering that optimize submodular coverage objectives (e.g., UCB) can achieve near-optimal performance [Srinivas et al., 2012, Binney and Sukhatme, 2012]. Adaptive or online IPP techniques can make use of discrete state spaces [Lim et al., 2016, Arora et al., 2017], known metric maps [Singh et al., 2009, Jawaid and Smith, 2015], unconstrained sensor placement [Krause et al., 2008b], or nonmyopic sensor placement [Flaspohler et al., 2019] in order to design trajectories through a potentially large state and vehicle space in order to gather useful observations.

In this work, we take an offline approach to informative path planning, and leverage the restriction of using uniform-coverage trajectory objects (e.g., lawnmowers) to relax the UCB reward function, setting β to 0. This effectively creates a purely exploitative reward function, which is tempered by external restrictions to the set of actions the robot can take. Under a different set of action primitives or online decision-making, utilizing the full UCB reward, or any of the other typical probability measures, would be suitable. Moreover, the computation of these information measures is directly supported by the PHUMES model class.

3.2 Plume Hunting with Robots

Unexplored. In the robotics literature, plume hunting has been equivalently styled as odor mapping, odor localization, source localization, and source seeking. In a large portion of these works, it is assumed that the source *location* is unknown, and through partial observations of emitted gas/odor/plume, the source can be discovered using techniques that can be divided broadly into biologically-inspired heuristic search (e.g., [Reddy et al., 2022, Chen and Huang, 2019]) or adaptive informative path planning (e.g., [Salam and Hsieh, 2019, Jakuba, 2007]). Biologically-inspired or heuristic techniques draw (varying-levels of) inspiration from animal or insect behavior in olfactory settings. Such techniques typically include gradient-based algorithms like chemotaxis [Morse et al., 1998], or bio-inspired algorithms that directly mimic a particular animal [Edwards, 2001]. These techniques are typically reactive and myopic, although they have been demonstrated to be relatively robust in open-world settings. In contrast, adaptive informative path planning can be nonmyopic, and typically attempts to embed knowledge (either heuristically or rigorously) about flow-fields (i.e., advection and diffusion) to assist in plume localization. Such techniques live on a spectrum, from algorithms that resemble biologically-inspired techniques like infotaxis [Vergassola et al., 2007] to methods that use model order reduction techniques (like proper orthogonal decomposition) to encode complex numerical models (like the Navier-Stokes equations) and elucidate spatiotemporal structures in complex data [Peng et al., 2014]. Some examples of specifically localizing hydrothermal plumes are presented in [Jakuba, 2007, Branch et al., 2020, Wang et al., 2020, Ferri et al., 2010].

In contrast to vent or source localization work, this paper aims to maximize samples collected throughout the structure of a moving plume in an offline information-gathering setting. Indeed, the plume source is generally known. Work that has used robots to map or chart plume-like structures has been presented as the “front-tracking” problem [Li et al., 2014]. In this problem, two water masses converge (say, at a river output into a bay), and the goal is to use a robotic vehicle to track the edge or intersection of these water masses using online adaptivity. With respect to tasking robots to stay within a particular water mass, most work has been conducted with multi-robot systems sharing distributed observations, and which identify key “neighborhoods” for further examination [Chen and Huang, 2019]. The importance of online decision-making in these schemes is essential to their efficacy; as far as these authors are aware, this paper is the first to attempt water mass tracking within an offline optimization strategy with a single agent.

We need to talk about
this paragraph. The reader
is going to ask: “Is this paper
on sensor placement? If so, why
are we saying this?”

Are these techniques
relevant? Possibly. So what
is some way?

3.3 Bayesian Inverse Problems

In approximate POMDP solvers, the choice of belief representation over the partially-observable state is critical for computing informative reward measures and simulating possible actions and observations in decision-making. Bayesian models are particularly well-suited to serve as belief representations because they enable inference over sets of unknown parameters informed by observations. A Bayesian inference problem takes the following general form: let $Z = \{z_0, \dots, z_{n-1}\}$ be a set of n observed data points (each a random variable, and each possibly a vector of values), X be the set of parameters that describe the data's distribution such that $z \sim \Pi(z|X)$, and α is a hyperparameter on the parameter distribution such that $X \sim \Pi(X|\alpha)$. Then the posterior distribution of the parameters given the data can be expressed as:

$$\Pi(X|Z, \alpha) = \frac{\Pi(X, Z, \alpha)}{\Pi(Z, \alpha)} \propto \Pi(Z|X, \alpha) \Pi(X, \alpha) \quad (5)$$

Practically, computing the posterior distribution exactly is computationally expensive or intractable due to the potentially large parameter space described by X , or complex hierarchical structure present between the observations and the parameter space. For the plume-charting problem, the Bayesian inference problem is posed as uncovering the state space S defined with parameter vectors x_p , x_c , and x_r from observations Z collected according to observation model O . In this instance, the observations, which are filtered binary measurements at particular locations, are related to the plume parameters x_p and crossflow parameters x_c via the complex spatiotemporal dynamics of plume physics, which can be represented as a systems of partial differential equations (PDEs).

To approximately solve Bayesian inference problems, techniques like variational Bayesian inference or Monte Carlo (MC) inference methods [MacKay, 1998] may be employed. MC methods estimate the true posterior by drawing samples from a proposal density and evaluating those samples with respect to the posterior. In large, complex systems, it is difficult to define a single density that well-describes a target posterior, and so Markov chain MC (MCMC) methods draw samples from a proposal density which is conditioned on the previous sample drawn, and establishing an acceptance criteria to transition between states [MacKay, 1998, Green, 1995, Neal et al., 2011]. Since each new state relies on the density of the previous state in MCMC samplers, a “burn-in” period, in which a potentially large number of samples are drawn, is used before virtually independent samples are generated. MC methods will converge to the true estimator of the posterior for large numbers of samples [MacKay, 1998]. In this paper, we make use of an MCMC procedure within our algorithm.

As the plume-charting problem is an informative path planning (IPP) task, it is worth noting that nonparametric Bayesian models like Gaussian Processes (GPs) [Browne et al., 2012] have enjoyed considerable adoption in IPP (e.g., [Flaspohler et al., 2019, Guestrin et al., 2005, Krause et al., 2008b, Srinivas et al., 2012, Luo and Sycara, 2018, Ouyang et al., 2014, Wan and Sapsis, 2017, Ma et al., 2017, Marchant et al., 2014]) to serve as the belief representation in POMDPs. GPs are attractive because they are relatively simply defined using a mean and covariance function (the latter of which encodes the “relatedness” of collected data with the inference target) and have a closed-form analytical update procedure. Unfortunately, challenges remain in adopting GPs for nonstationary and otherwise complex distributions present in realistic spatiotemporal environments. Recent work embedding numerical models into GP covariance kernels [Raissi et al., 2018], formulating general purpose nonstationary kernels [Singh et al., 2010, Garg et al., 2012, Chen et al., 2022], or utilizing learned latent spaces [Wilson et al., 2016] are promising areas for future adoption of GPs in spatiotemporal expeditionary IPP.

3.4 Buoyant Plume Physics

Fundamental to interpreting observations gathered during an AUV *Sentry* deployment and using them to quickly learn and improve a forward simulation of plume fluid location, is understanding the physics of plumes. Hydrothermal plumes in the deep sea are typically characterized as buoyancy-driven water masses. On formation at a vent site, emitted fluids are significantly less dense than background seawater (by virtue of being super-heated, with some additional effects from changes in chemical composition). This less dense water mass rises rapidly in the water column, forming

What is an inverse problem?
This section does not frame all we know how to do, and will the limitations on.

Need to connect this back to the other at hand.
 X includes the plume parameters, Z are the specific sensor requirements, etc.

Careful. Are these coming or semidef? Think of what a random variable, so should be a semidef?

State, not state space

This section has discussed IPP from previous paragraphs. IPP and GPs kind of come at the same time.

a *buoyant stem*. As a rule of thumb, a buoyant stem grows in diameter about 1 m for every 10 m vertically travelled. Due to rapid cooling, turbulent mixing, and the natural stratification of ocean water, vent-derived fluids will reach a point of neutral-buoyancy with the background seawater. At this point, the plume forms a *nonbuoyant or neutrally buoyant layer* which spreads out across the isopycnal that describes the ocean layer of equivalent density. In the Atlantic basin, plume rise height is typically expected to be approximately 300-350 m; in the Pacific basin, this is 150-200 m [Speer and Rona, 1989].

Generalized plume models which have been commonly incorporated in robotic source seeking literature include the Gaussian plume model [Green et al., 1980], and the Gaussian puff model [Ludwig et al., 1977]. These models primarily describe the dispersion envelope of aerosols released as a plume from a coherent source in the atmosphere, modeling the concentration of those aerosols directly as a Gaussian around a plume centerline describing the path of the plume in space. These models have largely been used to model ground pollution characteristics of smokestack-like sources in open, unstratified environments, and typically assume that the advective crossflow dominates plume movement. In the deep sea, weakly and strongly stratified environments are the norm, and buoyancy forces are the primary advective force of plume fluids, however the “Gaussian assumption” is widely accepted by physical oceanographers, and we utilize this assumption within our PHUMES framework. Specifically, we use deep sea suitable formulations of plume centerline dynamics, and apply the Gaussian assumption to the terms that describe space-averaged fluid characteristics. This yields numerical descriptions of buoyant plume “envelopes” in which plume-derived fluid masses, on-average, will be observable under consistent environmental conditions in time (that is, they are spatially-averaged models for a snapshot in time).

The buoyant-stem, neutrally-buoyant layer model of a hydrothermal plume has been mathematically codified perhaps most famously by [Morton et al., 1956] as a system of conservative equations (here for a stratified fluid) in cylindrical coordinates (x, r) with the x -axis vertical with the vent source at the origin:

$$\text{Volume: } \frac{d}{dx}(b^2 u) = 2b\alpha u \quad (6)$$

$$\text{Momentum: } \frac{d}{dx}(b^2 u^2) = 2b^2 g \frac{\rho_o - \rho}{\rho_1} \quad (7)$$

$$\text{Density deficiency: } \frac{d}{dx}(b^2 u g \frac{\rho_o - \rho}{\rho_1}) = 2b^2 u \frac{g}{\rho_1} \frac{d\rho_o}{dx} \quad (8)$$

where α is a proportionality coefficient which represents gross mixing (or entrainment) that occurs at the edge of a plume, $b = b(x)$ is the (symmetric) radius of the plume, $\rho = \rho(x, r)$ is density inside the plume, $\rho_o = \rho_o(x)$ is density outside of the plume, ρ_1 is some reference density such that $\rho_o(0) = \rho_1$, g is acceleration due to gravity, and $u = u(x, r)$ is vertical velocity. These equations have been equivalently expressed in terms of mass, salt, heat, and momentum conservation by [Speer and Rona, 1989] which usefully decomposes density into components of salinity and temperature which can be directly observed by scientific instruments.

In most environments, including the one we study in this paper, advective crossflow is present. This “bends” a buoyant stem and reduces the effective rise height of the plume by introducing more aggressive mixing. To describe the plume shape under crossflow, we reformulate plume ascension through a weakly stratified water column into a modified cylindrical coordinate system with along-the-plume-centerline axis s and centerline trajectory angle θ [Tohidi and Kaye, 2016]:

$$\frac{dQ}{ds} = Q \sqrt{\frac{2(1 + \lambda^2)}{M\lambda}} (\alpha \left| \frac{M}{Q} \right| - U_a \cos \theta | + \beta |U_a \sin \theta|) \quad (9)$$

$$\frac{dM}{ds} - U_a \cos \theta \frac{dQ}{ds} = \frac{FQ}{M} \sin \theta \quad (10)$$

$$U \sin \theta \frac{dQ}{ds} + M \frac{d\theta}{ds} = \frac{FQ}{M} \cos \theta \quad (11)$$

I had a hard time with his paragraph so I gave up
and we bring it back

$$\frac{dF}{ds} = -QN^2 \sin \theta \quad (12)$$

$$x_a = \int_0^s \cos \theta ds \quad (13)$$

$$h_a = \int_0^s \sin \theta ds \quad (14)$$

where $U_a = U_a(z)$ is the ambient crossflow velocity, $Q = Q(s, \theta)$ represents the plume specific volume flux, $M = M(s, \theta)$ is the specific momentum flux, $F = F(s, \theta)$ is specific buoyancy flux, N is the Brunt-Vaisala frequency, λ is the ratio of the minor and major axis that define the plume cross-sectional ellipse, x_a and h_a represents the Cartesian transform of s and θ within the plume's frame of reference, and α and β are vertical and horizontal entrainment coefficients. Indeed, the two key differences between this formulation and the formulation under no advective crossflow is the introduction of an additional mixing (entrainment) coefficient, and the tracking of volume, momentum, and buoyancy (density changes) fluxes horizontally under influence from this mixing. To convert abstract notions of buoyancy and momentum flux to directly observable ~~measured~~ vent characteristics like vent area or fluid exit velocity, which are expressed naturally in the non-advection model, we can use the following relationships:

Why the parentheses?

$$Q_0 = \lambda u_0 \frac{A_0}{\pi} \quad (15)$$

$$M_0 = Q_0 u_0 \quad (16)$$

$$F_0 = g 10^{-4} (T - T_0) Q_0 \quad (17)$$

where A_0 is the vent area, u_0 is the initial fluid velocity leaving the vent, T is the temperature of fluid at the vent, and T_0 is the temperature of ambient seawater at the depth of the vent (note that temperature is the dominant component of density, ρ , for deep sea hydrothermal plumes). Indeed, temperature, area, and exit velocity compose a sufficient set of parameters for representing the initial conditions of any particular plume and plume envelope calculation; these parameters, in addition to the mixing coefficients, form our set of x_p in \mathcal{S} in the plume-charting POMDP. U_a and the global heading of the crossflow, Θ_a (not directly modeled in these equations), form the parameters in x_c in \mathcal{S} .

Numerical models which describe instantaneous, complicated structure of plume phenomenon in time (e.g., [Lavelle et al., 2013, Xu and Di Iorio, 2012]) have been developed which enhance these spatially-averaged models by directly modeling partial derivatives with respect to time, and incorporating additional dynamical models such as the Navier Stokes equations. Given the computational complexity of these models (on the order of a day on a high-performance computing node to compute a single instance of the evolution of a plume for an hour), we instead focus on leveraging the comparatively simple and fast to compute “envelope” models described within PHUMES. We leave as future work opportunities to incorporate these more sophisticated models into expeditionary science missions and discuss further in Section 8.

4 Methodology

To solve the plume-charting POMDP as described in Section 2.3, we present a specific instance of PHORTEX, which utilizes a physically-informed probabilistic model (PHUMES) to generate forecasts of spatiotemporal distributions of plume fluids and optimizes chains of trajectory primitives (e.g., lawnmowers) to maximize the total number of observations of those plume fluids. PHORTEX iteratively improves the performance of these trajectory chains for each deployment of AUV *Sentry* using the history of collected observations from the robot's heterogeneous science sensors.

I don't know what it means!
Xylophone to be a cargo?
So clearly, And it will support
no a small job of almost same
primary, factors of temperature, and
chemical composition in the ocean.
So what?

4.1 Plume Detection: Treatment of Robotic Science Sensors

For any instance of PHORTEX, it will be necessary to process continuous measurements from multiple science sensors into a product that can be used to train the PHUMES model. For some combination of sensors and tasks, there may be a sensor for which the continuous signal can be directly used—for instance, using optical backscatter for finding the most densely populated algal patch—but in the hydrothermal charting task, there is no one sensor that can be used directly as a proxy for whether a parcel of fluid was hydrothermally derived [Jakuba, 2007]. This is due to the variable rates for which temperature, chemistry, and particulate matter persist within a plume structure. While temperature anomaly is a strong indicator for a buoyant stem, in the neutrally-buoyant layer temperature anomaly may be on the scale of noise of the sensor (only a few hundredths of a degree). Chemistry anomaly can persist longer within a plume, but is subject to unknown and variable rates of microbial digestion, and some chemical signatures can be tied to other oceanographic processes (such as mixing of stratified layers in the water column) that may be a false signal. Elevated particulate density can be a strong signal in the neutrally-buoyant layer for hydrothermalism derived from “smoking” vents, but not every vent will produce plumes with dense particulates. Taken together, this requires developing a sensing strategy that can fuse observations from multiple science sensors onboard AUV *Sentry* into a data product which can helpfully indicate whether the robot encountered plume fluids.

We elect to create a binary measurement indicating whether *Sentry* was in a plume or in background seawater. The following sensors are used to compute this measurement: conductivity probe (salinity), temperature probe (temperature), oxidation-reduction potential (ORP) instrument (relative “reactivity” of water), optical backscatter (OBS) instrument (turbidity), optode (oxygen), and experimental spectroscopic instruments Pythia and SAGE (dissolved methane). Sensors are internally logged at variable rates, but sub-sampled to a fixed 1 Hz sampling rate with a shared clock time for the purposes of directly comparing the instruments. Each of these sensors has its own physical characteristics and response to the chemistry of plume water. For example, ORP exhibits a large negative spike when first encountering plume water and then a slow hysteresis back to a nominal values. Measurements of salinity, temperature, and oxygen are expected to be influenced not only by plume water, but background physical mixing in the ocean; in contrast, turbidity, ORP, and methane are signals strongly associated with hydrothermalism because they are not persistent in typical seawater. To honor the different ways in which sensors respond to plume waters, an individualized processing regime is used for each sensor to detect “potential plume masses” in each stream (see Table 1), then weighted corroboration is used to ultimately classify each observation. Weights are assigned based on the relative “trustworthiness” of a sensor for plume classification, and a total corroboration score of 4 or more was used to classify an observation. An example of this sensor applied to real *Sentry* detections is shown in Fig. 2.

Quantity	Positive Plume Detection Criteria	Weight
Salinity	Detrended practical salinity outside 3 standard deviations of the entire time series	1
Temperature	Detrended temperatures above the 75th percentile of entire time series	2
ORP	Detections less than -0.005	2
OBS	Optical attenuation above the 75th percentile of entire time series	2
Oxygen	Detrended concentrations outside one-hour rolling computation of 3 standard deviations	1
Methane	Normalized concentration above 0.3	2

Table 1: Instruments on AUV *Sentry* and the criteria used to identify plume fluids for each instrument. The weight is used to indicate relative “trustworthiness” of a plume detection for each sensor, and is used in a corroboration scheme that sums detections across sensors in order to make a final determination on whether an observation location contained a parcel of plume fluid or consisted of background seawater. “Detrending” data removes depth-related cross-sensitivity from the measurements; for example, temperature is stratified in the deep ocean, so to ignore the impacts of depth changes in the data stream, those effects are removed by “detrending” the data stream.

This approach for processing complex sensor observations into binary plume detections was initially developed by Jakuba, [2007]; our method is an adaptation of the process using recommendations from this previous work and in consultation with the science team we were directly collaborating with for this study. The result of our sensor model is to convert multiple, time-stamped sensor observations $s_{t,i} \in \mathbb{R}$, $i = 1, \dots, S$ to a single, binary plume-detection $z_t \in \{0, 1\}$. These binary plume detections are then used to update our plume model and plan robot trajectories, as described in the following sections.

Do we have any way to assess the accuracy of this sensor model?

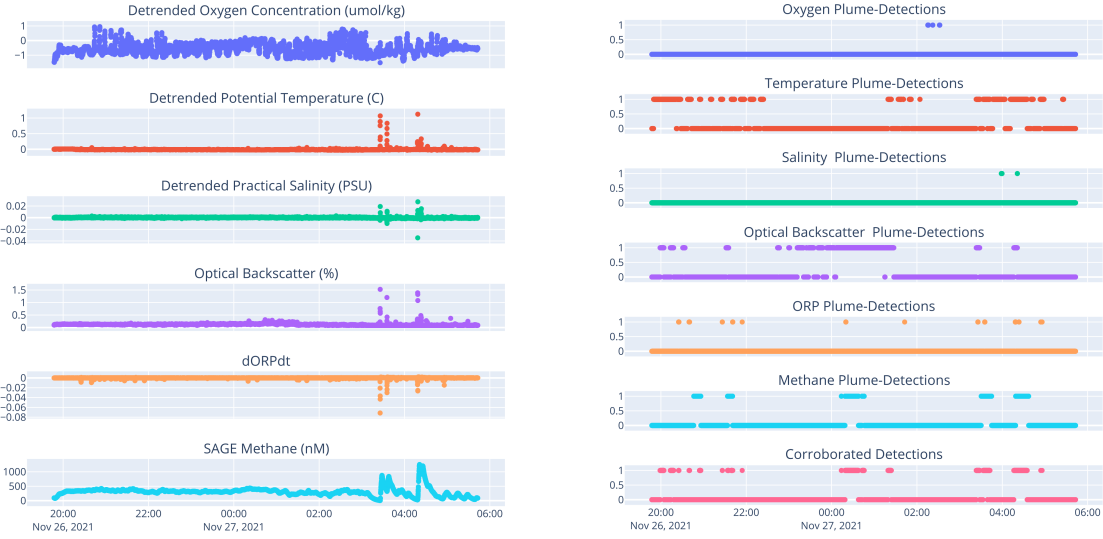


Figure 2: Example time series (left) and associated detections (right) over the AUV *Sentry* sensor suite. Oxygen, temperature, and salinity measurements are detrended using a linear transformation fit to depth vs. value plots. The time series demonstrates two types of plume detections. The first are “obvious detections” in which most sensors register strong anomalies (this happens twice toward the end of the deployment) and are most strongly associated with buoyant-stem derived fluids. The second are “persistent-plume detections” in which the robot traverses through water that is slightly more turbid, warm, or chemical-rich than background water over potentially long horizons (this happens early in the deployment and in the middle). Such detections are most strongly associated with neutrally-buoyant layers. The conservative corroboration detector successfully identifies both forms of plume water.

4.2 External Sensing: Leveraging All Available Information

Outside of AUV *Sentry*, several sensing packages were deployed during the research cruise which collect relevant information about the state of temporally evolving crossflow and ambient seawater properties. We leverage these external measurements within our PHUMES instance in two ways: (2) setting default seawater constants of the target site, and (2) to learn the crossflow transition function T_c .

On the first point, external sensors were used to define the stratification curve of the Guaymas Basin water column. This information is used within the physically-informed layer of PHUMES and treated as a constant throughout the expedition. This information could be equivalently extracted from sensors onboard *Sentry*, but the available external sensing package was higher fidelity for the purpose of water column characterization. Moreover, as this information is not explicitly reasoned over for the purposes of plume-charting (as it can be observed once and assumed to be effectively constant), it is convenient to incorporate this information outside of the sequential decision-making process.

On the second point, critically there was no “current sensor” on *Sentry* available during our expedition that could be used to measure the *in situ* current magnitude and heading during a deployment. While it may be possible to estimate T_c solely from the binary observations as defined in the preceding section, access to an external bottom-mounted sensor (tiltmeter) on the seafloor during this expedition significantly relieved the burden of this inference process. We learn T_c by fitting a Gaussian process (GP) with composite radial-basis-function and periodic kernel functions to point observations of crossflow magnitude and heading observed by the tiltmeter. Approximately 3 days of observations were available for training. Once the GP was trained from external data, crossflow parameters \mathbf{x}_c in \mathcal{S} were set with the expected mean of the GP. Presently, a crossflow sensor is in development for *Sentry* using existing acoustic technology onboard the robot; in such a configuration, the process of estimating T_c would be dependent on robot actions and would be a less independent process to the plume-charting task.

Need to be clear about what function is being learned by the GP.

4.3 PHUMES: Physically-informed Probabilistic Forecasts

PHUMES is a model class that can generate predictions of the distribution of a spatiotemporally evolving state from a history of sparse state-space observations. To quickly learn a predictive model of a spatiotemporal phenomenon, PHUMES leverages access to analytical scientific simulators (when available) codified as systems of ordinary differential equations (ODEs). These simulators reduce the dimensionality of the inference problem from the full-state of the environmental phenomenon (e.g., a 4D volume in space and time with continuous phenomenon measurement) to the dimensionality of the initial conditions and meta-parameters of the simulator (which can then be used to populate the full-state for planning purposes). The use of ODE systems, as opposed to high-fidelity numerical simulators ~~of~~ ^{using} partial differential equations (PDEs) is intentional; the computational requirement of most PDE systems used to model environmental phenomenon at the scales studied during expeditionary missions ~~is~~ ^{are} practically intractable. In contrast, ODE systems are less well-resolved, but summarize the structure of an evolving phenomenon in a useful way that can be enhanced by a generic probabilistic formulation wrapping the ODEs.

At a high-level, PHUMES consists of two key phases: forecasting (forward simulation) and updating (inverse problem) (Fig. 3). In the forecasting step, samples from the distributions of the initial conditions and meta-parameters of the simulator are pushed through the simulator to form a composite distribution in the full state space of the target phenomenon. Time is discretized over domain-specific key points, and any parameters reliant on time are sampled at those discrete points. This creates a forecast that is essentially a series of “snapshots” of the phenomenon. The forecast is provided to a trajectory optimizer for planning. While the robot is executing a plan or following the execution of a plan, PHUMES performs an update of the initial conditions and meta-parameters from observations. The specific choice of update procedure is dependent on the exact form of the observations available, however to leverage the simulator in the update step we use (and recommend) an MCMC procedure. In this scheme, collected observations are compared directly with the simulated output of samples over the parameters to be updated, and the posterior over these parameters are updated by stochastically accepting or rejecting samples weighted by the agreement between the observations and simulation. For any inference targets of interest that may not be well captured by a simulator, parallel inference models (e.g., Gaussian processes, particle filters) could be used.

In the plume-charting POMDP as formulated, PHUMES is updated following each deployment of *Sentry*. For a single deployment, upwards of 20,000 observations may be available (each deployment is a minimum of 6 hrs in duration, up to 24 hrs, and sensing is logged at 1 Hz). The total number of deployments at a single site is typically small (less than 5, and perhaps more typically less than 3), so maximizing the “return” of each deployment to plan the next is critical. AUV *Sentry* provides observations of binary plume detections and continuous crossflow magnitude and heading, $Z = [\{0, 1\}, \{\mathbb{R}^+\}, \{(-180, 180]\}]^n, n \in \mathbb{Z}^+$. In the inference procedure, we would like to update estimates of our state \mathbf{x}_p and \mathbf{x}_c . The simulator available to us is defined by a model of buoyant plumes in crossflow, defined in Section 3.4. The initial conditions and meta-parameters of this simulator are vent area, vent fluid temperature, vent fluid exit velocity, horizontal mixing coefficient, vertical mixing coefficient, global current heading (at a moment in time), and global current magnitude (at a moment in time). Thus, the exact composition of \mathbf{x}_p and \mathbf{x}_c reflect these values. We initially place an uninformative prior over these vectors, $\Pi(\mathbf{x}_p)$ and $\Pi(\mathbf{x}_c)$ and aim to ^{inform} learn the posterior distributions $\Pi(\mathbf{x}_p|Z)$ and $\Pi(\mathbf{x}_c|Z)$ ¹.

At the forecasting step, PHUMES generates a time-indexed $t \in T$ composite estimate of the distribution of plume fluid in a 3D volume $\bar{\mathbf{W}}$ by forward simulating time-dependent M samples of the states $x_{p,t}^{(m)} \sim \Pi(\mathbf{x}_p(t))$ and $x_{c,t}^{(m)} \sim \Pi(\mathbf{x}_c(t))$ through the plume simulator $f(\cdot, \cdot)$:

$$\bar{\mathbf{W}}_t = \frac{1}{M} \sum_{m=1}^M f(x_{p,t}^{(m)}, x_{c,t}^{(m)}) \quad \forall t \in T. \quad (18)$$

¹We effectively separate inference over \mathbf{x}_p and \mathbf{x}_c given the observation model available; indeed we assume that observations of crossflow can be treated as independent of observations of plume detections. This is strongly supported in the practical deployment of *Sentry*, when an external sensor was necessary to observe crossflow. If instead the sensors were co-located on *Sentry*, inference over the joint posterior $\Pi(\mathbf{x}_p, \mathbf{x}_c|Z)$ could be done instead.

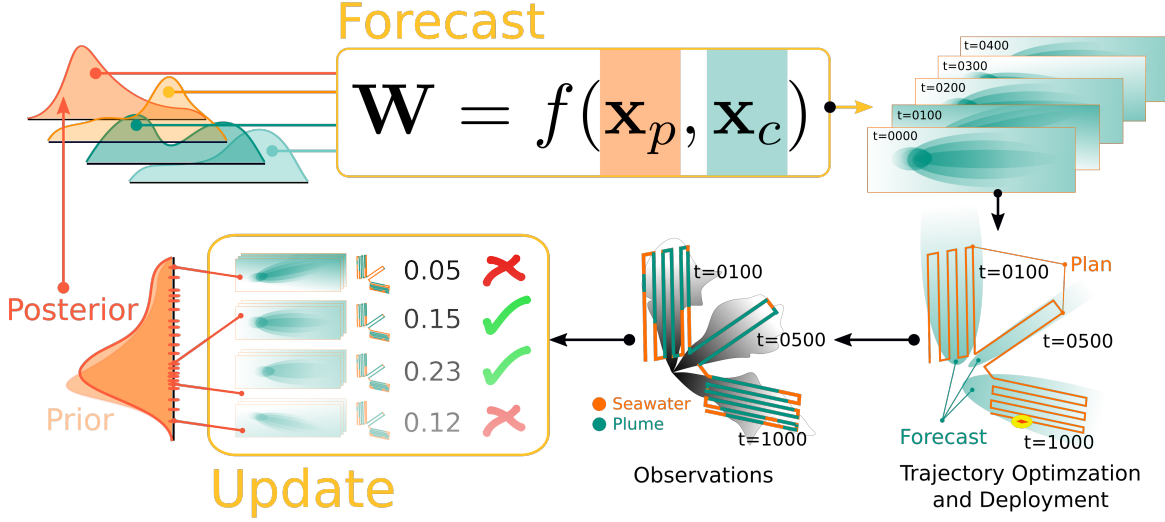


Figure 3: PHUMES: **P**Hysically-informed **U**ncertainty **M**odels for **E**nvironment **S**patiotemporality; a model class for forecasting spatiotemporal distribution evolution trained on partial observations. PHUMES generates forecasts by leveraging an embedded analytical model $f(\cdot, \cdot)$ that approximates the physics-driven evolution of a target distribution. This model is seeded with many samples from distributions placed over initial conditions, physical parameters, or temporal functions (such as \mathbf{x}_p and \mathbf{x}_c here). The composite result of this process is a forecast \mathbf{W} that consists of a mean and variance of phenomenon occupancy in a 3D volume over snapshots of time. This forecast is provided to a trajectory optimizer which sets a deployment trajectory that is executed by a robot. The deployment generates a series of observations, which are then used to update the distributions of the generating distributions via an MCMC procedure which compares the gathered observations with the simulated observations of samples from the generating distributions. The resulting posterior update over the generating distributions is then used for the next planning iteration.

The complete forecast $\bar{\mathbf{W}}$ is then used by a trajectory optimizer to approximate the reward function $R([\mathbf{x}_p, \mathbf{x}_c]^T, a) = \mathbb{I}[\text{in_plume}(\mathbf{x}_p, \mathbf{x}_c, \mathbf{x}_r, a)] \approx \mathbb{I}[\text{in_plume}(\bar{\mathbf{W}}, a)]$. Equivalently, \mathbf{W} is the robot's belief b . The variance of the forecast $\mathbf{S}_{\mathbf{W}}^2$ can be similarly computed, depending on the requirements of the reward function.

At the update step, the distributions over \mathbf{x}_p and \mathbf{x}_c are updated from observations Z collected by *Sentry* (and/or external sensors). To find $\Pi(\mathbf{x}_c|Z)$ we use GP models for crossflow magnitude and heading as described in the preceding section. A bulk, closed-form analytic update is made to the GP parameters following typical implementations [Browne et al., 2012]. For $\Pi(\mathbf{x}_p|Z)$, we use a random-walk Metropolis-Hastings MCMC method [Metropolis et al., 1953] to perform the update. Simulations of deployments are generated by samples of \mathbf{x}_p and \mathbf{x}_c pushed through $f(\cdot, \cdot)$ and are compared with the collected binary observations. Samples of \mathbf{x}_p are then stochastically accepted or rejected, weighted by agreement between simulated and true observations. In practice, we use a likelihood model which sets a false positive and false negative rate assigned by intuition of the sensing performance of *Sentry*; in this work we set the false positive rate to 0.1 and the false negative rate to 0.3. As this inference method is a chaining procedure, the next samples of \mathbf{x}_p are informed by the previous, and with enough samples, the cumulative distributions of accepted samples are guaranteed to converge to the true underlying distributions for each of the elements in \mathbf{x}_p . For the following deployment, the posterior is set as the new sampling distribution for forecast generation.

4.4 Trajectory Optimization for Path Planning with Fixed Primitives

To solve the plume-charting sequential decision-making problem, we begin with the POMDP value function Eq. (4) and introduce the model defined in Section 2:

$$V_h^*(b) = \max_{\{\theta_1, \dots, \theta_n, n | \theta_i \in \Theta, n \in \mathbb{Z}^+\}} \mathbb{E}_{[\mathbf{x}_p, \mathbf{x}_c, \mathbf{x}_r]^T \sim b} [R([\mathbf{x}_p, \mathbf{x}_c, \mathbf{x}_r]^T, \{\theta_1, \dots, \theta_n\})] \quad h \in [0, H-1], \quad (19)$$

where $\theta \in \Theta$ parameterizes individual trajectory primitives in a length- n sequence of chained trajectories and b is the planner's belief about the state of the plume, currents, and robot, and the discount factor γ has been set to zero to encode our single-dive planning approximation. Solving Eq. (19) still involves the challenging optimization of n trajectories and the joint optimization of all n trajectories into a chain. To simplify the planning problem, given the constraints of real-world robotic deployments, we assume that the number of chained trajectories is given, i.e., $n = N$, and that each trajectory can be optimized independently. This results in the following approximation:

$$V_h^*(b) \approx \max_{\theta_1 \in \Theta} \dots \max_{\theta_N \in \Theta} \mathbb{E}_{[\mathbf{x}_p, \mathbf{x}_c, \mathbf{x}_r]^\top \sim b} [R([\mathbf{x}_p, \mathbf{x}_c, \mathbf{x}_r]^\top, \{\theta_1, \dots, \theta_N\})] \quad h \in [0, H - 1]. \quad (20)$$

We solve Eq. (20), which defines multiple, independent, non-convex, constrained optimization problems, using the trust-constrained method in the `scipy` optimization library for a fixed number of iterations [Conn et al., 2000]. To evaluate the reward function $R([\mathbf{x}_p, \mathbf{x}_c, \mathbf{x}_r]^\top, \{\theta_1, \dots, \theta_N\})$, we define a trajectory sampler operator $\mathcal{G} : \Theta \rightarrow \mathbb{R}^{3 \times k}$ that takes a trajectory parameter vector as input and produces a set of locations in \mathbb{R}^3 that will be sampled when the robot executes the trajectory, where k is the number of sampled points. These sample points can then be compared with the plume forecast \mathbf{W} produced by PHUMES to count the number of sample points that are contained within the inferred plume.

In practice, we choose our trajectory class to be a lawnmower trajectory, which were parameterized by a vector θ that determines the origin, orientation, height, width, and resolution of the lawnmower. The trajectory sampler \mathcal{G} produces the lawnmower specified by θ and then subsamples uniformly along its length. We defined the set Θ to enforce that the lawnmower trajectories are contained within a pre-defined, rectangular safe region and that each lawnmower obeys a time-based budget constraint.

4.5 At Sea Operations

When performing field operations on the research vessel with AUV *Sentry*, we used PHORTEX to enable deployment-by-deployment autonomy that could iteratively improve robot performance with each deployment (Fig. 4). Functionally, the trajectories planned with PHORTEX were provided to the *Sentry* engineering team for extensive safety validation prior to each deployment. If approved by the *Sentry* team, the chief scientist, and captain of the vessel, the trajectories were downloaded into the *Sentry* mission planning software as static waypoints. This confirmation process required a lead time of approximately 6 hrs before a given deployment time, and approximately 12 hrs were available between deployments to mechanically service *Sentry* and recharge batteries. The ability of PHORTEX to produce viable trajectories from data within the first 6 hrs that *Sentry* was on-deck following a recovery was critical for keeping this strict timeline. Given the long lead time between trajectory design and *Sentry* deployment, there were many opportunities for the time of a deployment to change due to developments in weather, other science/technology priorities, a critical personnel was occupied, etc. To be robust to these changes, we provided deployment plans that started several hours before and several hours after a given deployment time, and the *Sentry* team truncated the plan at the appropriate point once a deployment time was known with certainty.

5 Field Deployment: Charting Deep-Sea Hydrothermal Plumes

In November 2021, a research cruise aboard the Research Vessel (R/V) *Roger Revelle* was conducted to the Northern Guaymas Basin in the Gulf of California to study a recently discovered hydrothermal ridge [Soule et al., 2018, Geilert et al., 2018]. The research cruise had several objectives: test novel *in situ* instruments to measure dissolved methane, test novel *in situ* instruments to measure the carbonate cycle, map the heat distribution in shallow sediments above hydrothermal sills, collect specimens of tubeworms, and collect biological samples of microbiota in hydrothermal plume-fluids for *ex situ* analysis to re-construct the structure of a plume microbiome. It is typical that research cruises have several science teams working together under an appointed chief scientist to maximize the use of ship assets while at sea. To assist in operations, AUV *Sentry*, remotely-operated vehicle (ROV) *JASON*, and standard oceanographic acoustic and profiling equipment were available. The deployment of PHORTEX on the cruise for *Sentry* operations was

Separate & Validating
the information

This description is how
itself, and feels ad hoc.

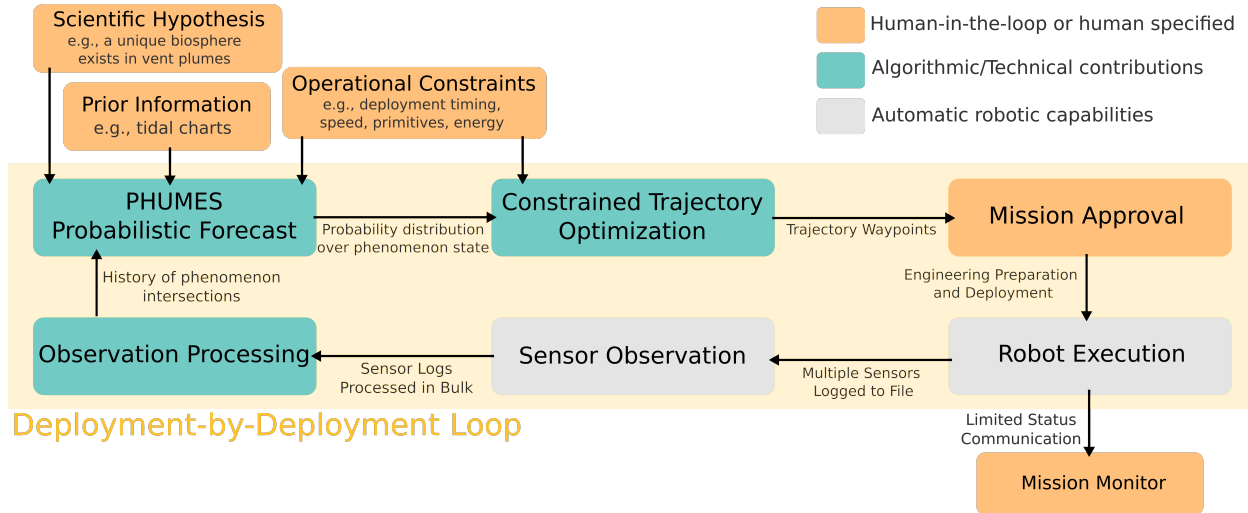


Figure 4: The at-sea operations implementation of PHORTEX. Integration of scientific knowledge, prior information, auxiliary sensor information, and operational constraints was done at the initialization of the PHORTEX deployment-by-deployment loop. Every trajectory generated by PHORTEX was checked by AUV *Sentry* engineers and the science team before execution. *Sentry* status was monitored with an external acoustic tracking system that monitored vehicle location, power, and performance while in acoustic range of the ship. Upon returning to deck, all science sensor observations were downloaded in bulk from the vehicle, and then ingested via our PHORTEX system.

coupled with objectives to test *in situ* instruments and collect microbiota samples. For both of these tasks, charting different regions within a plume structure was important to test the limits of the novel instruments and collect microbiota samples from a diversity of plume-conditions.

5.1 Site Description and General Conditions

The main site for the study conducted by AUV *Sentry* using PHORTEX is a hydrothermal ridge located in the northern Guaymas Basin, approximately 1850 m underwater and at the edge of an additionally 300 m deeper graben (a valley with steep sides) (Fig. 5). The ridge is approximately 600 m long and features several tall sulfide structures 45–75 m in height with active smoking along their bodies. A smoking “chimney” at the northernmost point of the ridge was targeted for plume-charting. Composed of a cluster of tens of small orifices (<0.1 m diameter) creating an approximately 1.5 m diameter chimney base, the fluid produced was thick with particulate matter, 340 °C at the source, ventilated rapidly at approximately 0.7 m s⁻¹ (as measured by video equipment), and rich in dissolved methane. In contrast, the ambient seawater was methane-poor, considerably less turbid, and cold at 4 °C. Vent characteristics were measured by ROV *JASON* carrying specialized sensing equipment, and we use these measurements as a means of seeding and measuring the performance of PHUMES within PHORTEX.

As vent fluids rise and form a plume at this site, the ambient water is mixed (entrained) at an unknown rate. The presence of advective crossflow, reaching magnitudes up to 0.1 m s⁻¹, was obvious from images of the bending plume stem at the vent sites (and was measured by the bottom-mounted tiltmeters deployed during the expedition). The magnitude and heading of the crossflow appeared to be semi-cyclic, following a pattern (albeit time-delayed) established by tidal charts produced by Centro de Investigación Científica y de Educación Superior de Ensenada (CISESE) for the time period of the expedition². Local bathymetric and other physical effects on crossflow were also qualitatively observed. Under these conditions, plume expressions could be transported several hundred meters from a known source, and would be expected to rise over 200 m in the water column. In scientific work following this expedition, plume fluids were identified from collected observations over 7 km away from known venting sites [IN PREP].

²charts available from predmar.cicese.mx/calendarios
Should be a direct URL

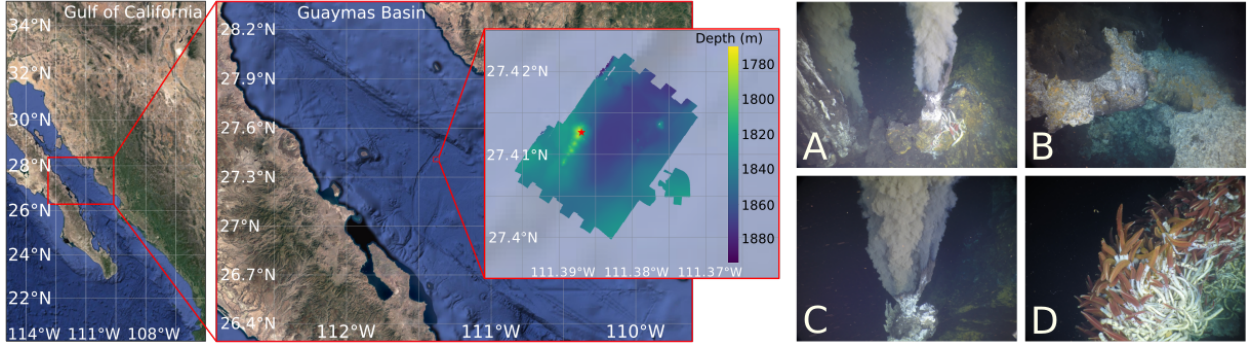


Figure 5: Study site in the Guaymas Basin, Gulf of California. The inset map is bathymetric data collected by AUV *Sentry* during this expedition and shows the approximately 600 m long ridge in yellow. The red star marks the chimney that was of particular study in this article. Pictures A-D show imagery from the ridge and chimney site. A-C show various forms of plume-producing vents located at the chimney and D shows an example of the macrofauna covering the structures along the ridge.

5.2 Overview of Sea Trials with AUV *Sentry*

Four deployments as part of the PHORTEX study were made with AUV *Sentry*, and represent a planning “spectrum” from fully human-designed surveys to fully PHORTEX designed. The intent of this was to compare standard survey techniques with PHORTEX. We refrain from claiming whether one methodology is better than the other, but instead aim to show the characteristics of each strategy as observed in this study. In Section 6 more quantitative claims about PHORTEX are made.

We label the four deployments as follows:

- **Dive H-Multi:** human designed, multi-task survey. This was the first deployment of *Sentry* and the survey was designed to both attempt to find plume fluids and to bathymetrically map the local basin area (the map of which would be used as part of the safety check protocol for future deployments). This dive is representative of a standard “nested” strategy, in which progressively more targeted (finer resolution) surveys are used to study areas that might be of interest. The deployment lasted 21.3 hrs and collected 76,604 observations total.
- **Dive H-Plume:** human designed, plume-charting survey. This was the second deployment of *Sentry* and the survey was hand-designed by the science party onboard the vessel to find and sample plume fluids. The science party had access to the performance of *Sentry* in Dive H-Multi. The strategy was to sweep the basin above areas with known hydrothermal vents, and fly out into the basin in the direction that the plume fluids would be expected to advect. The deployment lasted 21 hrs and collected 75,430 observations total.
- **Dive HP-Plume:** hybrid human and PHORTEX plume-charting survey. This was the third deployment of *Sentry* and the survey consisted of trajectories designed by PHORTEX trained by observations collected in Dive H-Multi. Two of the trajectory primitives designed by PHORTEX were replaced by “naive” lawnmowers placed over the known vent at two different times in the deployment. The deployment lasted 22.2 hrs and collected 79,792 observations total. Of these, 8.2 hrs and 29438 observations were collected via the naive strategy.
- **Dive P-Plume:** PHORTEX plume-charting survey. This was the fourth and last deployment of *Sentry*. The survey was fully designed by PHORTEX using observations from Dive H-Multi. The deployment lasted 9.9 hrs and collected 35,755 observations total. This deployment is notably much shorter than the other deployments due to increasing time constraints as the expedition was coming to a close. This deployment also used *Sentry* in a “depth-hold” mode; whereas in all other dives *Sentry*’s depth followed the basin terrain, in this experiment the robot held an absolute depth.

5.3 Experimental Results

We look at several key metrics for each deployment: proportion of positive plume observations, utilization of spatial extent, and utilization of temporal window. The first metric, proportion of positive plume observations, is simply the number of observations collected in a dive that were classified as in-plume by the binary psuedo-sensor we describe in Section 4.1. The second metric attempts to show how effective the design of the survey was spatially by first showing the absolute range that positive detections were made as a measure of distance from the chimney vent location and second showing how that range fit with the overall design of the survey. For example, if detections were made up to 300 m away from the vent, but the robot traveled up to 1 km away, then the survey spent too much time outside of the detectable plume region and would not be as effective as a survey that only traveled 200 m away but stayed well within the detectable plume range. Finally, the last metric is a measure of how effective the survey was at *staying* or *revisiting* a plume over time. Given the duration of these missions, it is important to use the entire mission window for the task at hand; moreover temporally “diverse” observations are of scientific interest generally. We report the dive hours with at least 10% or more positive detections.

A summary of these metrics for each dive is provided in Table 2 and visualized in Fig. 6. In general, we see that PHORTEX performs as least as well as the human-designed surveys in terms of total number of samples collected, while improving spatial utilization (both with respect to effective utilization of the entire explored range, and in terms of increasing the effective detection range over naive trajectories placed “on top” of the vent). Absolute temporal utilization is similar to human surveys, however the distribution of detections within the temporal utilization windows is potentially improved—for human surveys, detections tend to be “bunched” to either the first half (as in H-Plume) or second half (as in H-Multi). Anecdotally, in HP-Plume, the two human-designed surveys occur in hours 5-8 and 20-23. While there were detections in both of these windows, over 90% of total positive detections by these trajectories were collected only in the window from hours 20-23; in contrast the proportion of positive samples in the PHORTEX designed trajectories in HP-Plume were more uniformly distributed in time (approximately 40% collection in each window).

Dive	Duration	Total Obs.	Prop. In-Plume	Spatial Util.	Temporal Util.
H-Multi	21.3 hrs	76,604	22.3%	300 m (19%)	9-17,20-21 (52%)
H-Plume	21 hrs	75,430	10.9%	900 m (64%)	2,5-8,10-11,15-16 (43%)
HP-Plume	22.2 hrs	79,792	41.8%	600 m (100%)	1-3,5,7,11-23 (81%)
HP-Plume (H)	8.2 hrs	29,438	42.3%	250 m (100%)	5,7,20-23 (75%)
HP-Plume (P)	14 hrs	50,354	41.5%	600 m (100%)	1-3,11-20 (93%)
P-Plume	9.9 hrs	35,755	12.8%	450 m (100%)	1,5,8,9 (40%)

Table 2: Per-deployment statistics for field trials of PHORTEX. The deployment HP-Plume is broken further into human designed (H) and PHORTEX designed (P) portions for direct comparison.

In this field deployment it is obvious that PHORTEX could be a useful tool for plume-charting. The performance of trajectories designed with PHORTEX are comparable to those designed by humans with key possible improvements in spatial and temporal utilization. Moreover, the automated nature of PHORTEX operationally alleviates significant decision-making burden on a science team and the trajectory-design burden on the *Sentry* team; the ability to ingest data from external sensors and previous *Sentry* missions, and produce trajectories that can be seamlessly ingested by the safety checking system without human intervention is of considerable benefit when actually in the field. Moreover, the intermediate products of PHORTEX, such as PHUMES forecasts, are operationally useful for other tasks in field operations, such as deploying other instruments or prioritizing instrument deployment order based on temporal changes in the environment.

6 Validation in Simulation

[TODO: This section is under significant development; an outline of the intended content is provided.]

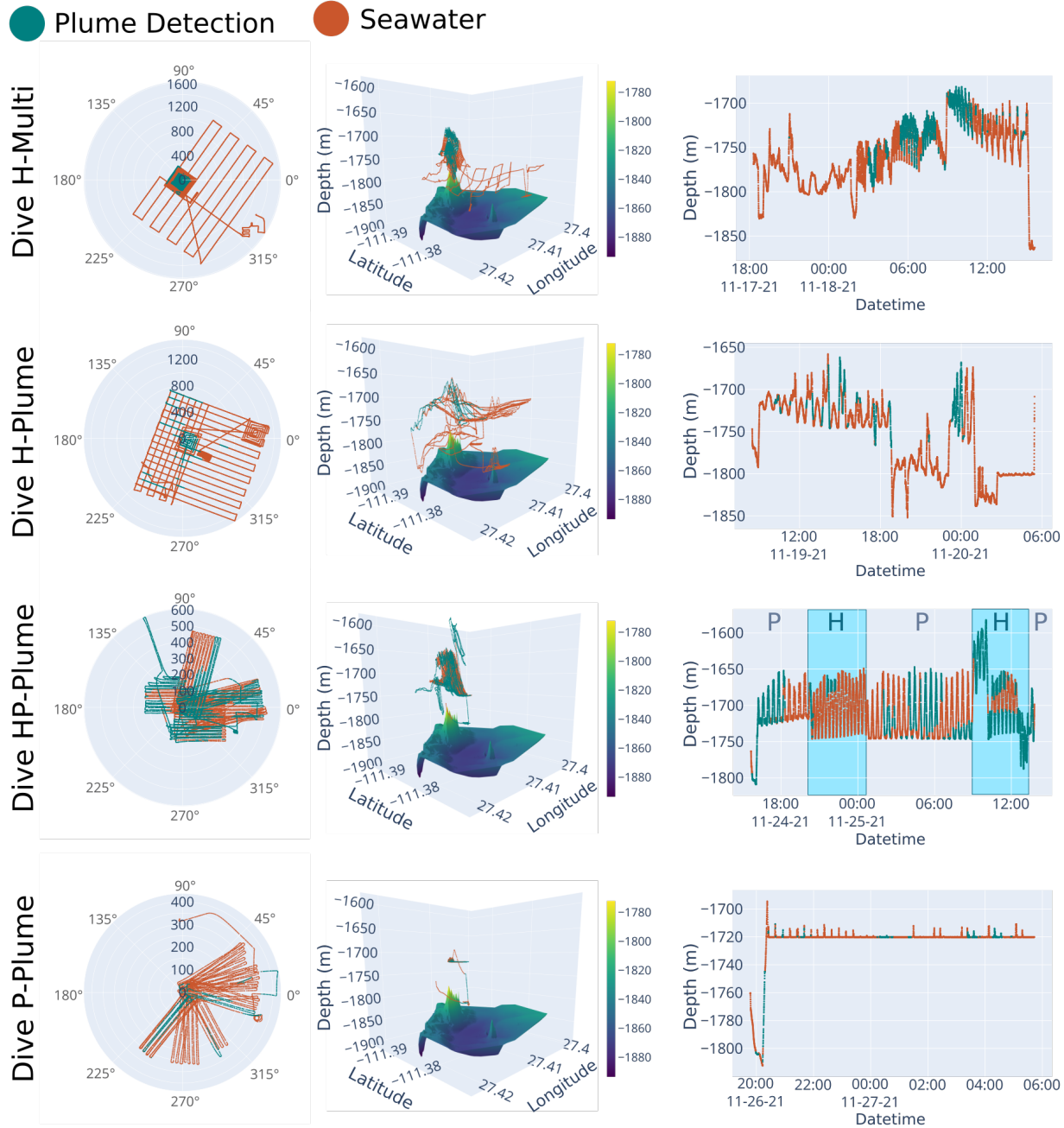


Figure 6: The four field dives of AUV *Sentry*. All data is plotted according to its detection identity (in-plume or seawater). The first column shows a top-view of the dive trajectories in polar coordinates, in which angle and radius is computed relative to the chimney coordinate of the vent of study. In the center column, the 3D path of the vehicle over the rendered bathymetric terrain is provided. All but Dive P-Plume were dives conducted in altitude-hold mode with *Sentry*, and so the trajectories show obvious changes in elevation; in contrast Dive P-Plume was held in depth-hold mode, so most observations are gathered within a depth-plane. The final column shows a time series versus depth of the detections collected. In Dive HP-Plume the portions of the dive that were human-designed and PHORTEX-designed are labeled with H and P, respectively. As can be seen in the Dive HP-Plume time series, the two human-designed trajectories have significantly different performance, despite being in locally similar regions of the spatial domain.

- We will first demonstrate PHORTEX within the simulator we've created for generating plume funnels. We will show how PHUMES converges to estimates of the true underlying distributions of initial conditions and parameter settings with and without noise. We will ideally show a graph that is RMSE of params versus mission iteration, and show a steep drop in error with steady improvement as iterations increase (fewer than 10 iterations will be graphed).
- We will additionally show performance on several key metrics, including reward versus iteration, total in-plume samples/accumulated reward under different model settings (e.g., number of samples in PHUMES MCMC chain, prior uncertainty), and model mean and variance with each iteration.
- We will then show how sensitive trajectory optimization settings/chains are to collected reward, intending to show the advantage of using chains over a single highly-resolved lawnmower, at minimum.
- If there is interest/time, we will then show how PHORTEX performs in a numerically realistic simulator (as provided by our collaborator at University of Washington) and compute similar statistics as those indicated above. This addition would be used to demonstrate the complex real-time structure of plume snapshots, and show how the method generalizes to this setting. *VP: note that this is only if there is time; currently planning on only using the field results to demonstrate this, and may save simulation work for later tag-along conference/workshop paper.*

7 Discussion

7.1 Lawnmower Actions and Exploitative Reward

In adaptive sampling and informative path planning research, defining the balance between exploration and exploitative actions is a consistent challenge. In this study, the operational restriction to use only uniform-coverage action primitives (lawnmowers) was leveraged to define a solely exploitative reward function (maximizing the sum of expected detection samples). Using the action space and reward definition in synchrony to achieve an explore-exploit balance for informative path planning has not necessarily been rigorously studied; however, the idea of chaining uniform coverage trajectories for adaptive search has been examined in [Mason et al., 2020] for hydrothermal vent localization. **[TODO: I think GF will have something interesting to add here!]**

7.2 Using Snapshots of Idealized Plumes

The PHUMES forecast provides a series of plume “snapshots” for trajectory optimization, in which these snapshots show the distribution of samples of idealized envelopes in which plume fluids may be present. By discretizing over time, these snapshots naturally do not capture the effects of advection and mixing of pre-existing plume fluids in a target water volume (that is, the snapshot from $t = 0$ does not influence the snapshot of $t = 1$ because the persistence of the fluids from $t = 0$ is not modelled directly). For the purposes of plume charting, it would be advantageous to have a more sophisticated model of plume-fluid persistence and continuity over time in order to better constrain the spatiotemporal coordinates of a particular observation. For this sophistication to be added, two key innovations would be necessary: a suitable analytical model and a suitable observation scheme.

The analytical model used here is among the most simple models for buoyant-plumes that express the impact of crossflow on the buoyant stem and neutrally-buoyant layer. To better model persistence, adapting Gaussian puff models [Ludwig et al., 1977] to better model the physics of buoyant plumes may be appropriate (although these models will similarly suffer from the persistence problem in some challenging environments in which basin scale “sloshing” caused by tides or other effects create unique mixing dynamics). When considering persistence, it also becomes increasingly important to model non-conservative properties of a plume, such as biological nutrient consumption or particulate deposition. As models of these phenomenon are active areas of research (as is developing more sophisticated plume models), it is obvious that working with domain experts to formulate the right physically-informed model for PHUMES is critical. Additionally, integrating other probabilistic tools to approximate/estimate unmodeled characteristics of an

environment by the analytical model could be utilized. These would be particularly well-suited to online planning domains, in which forecasts from an analytical model could be used e.g., to set the prior of a GP, and then live observations could be incorporated in real time for course correction while actually underway.

The observation scheme for a particular implementation has considerable impact on the sophistication of the inference that can be accomplished. In hydrothermal plume charting, there are heuristics for particular sensors that we employed to create a simplified binary data product; however a similar scheme could be used to develop a more continuous measure of the “plume-quality” of a particular water sample, or a learned sensor could be developed which could potentially create a more expressive data product. One of the challenges with environmental domains is the access to enough training data to create such learned sensors. But perhaps the larger challenge is simply the quality of the data available at large—much of the carbonate and other biogeochemical systems of environmental interest have either a limited or nonexistent selection of (*in situ*) sensors available to measure them. Of the sensors that exist, particularly for deep-sea work, the time-response of gas sensors is on the order of half-an-hour or longer (in this work, we made use of experimental sensors in active development with faster response times suitable for mobile AUVs). As the sophistication of sensing equipment improves, so too will the inference abilities of decision-making systems like PHOREX.

7.3 Compensating for Onboard Sensing Limitations

Leveraging sensing equipment external to a robot is well established for environmental studies in which satellite, observatory, or historical observations are available. However, in many environments—subsea, subterranean, forests—such observational equipment may not be available or needs to be independently deployed for a particular study by a science team or by a robot explorer. The use of multiagent systems for environmental studies in spatiotemporal fields (e.g., [Salam and Hsieh, 2019]) is particularly powerful, as robots can specialize in different sensing forms and collect simultaneous observations in different spatial locations. In this study, we leveraged an external crossflow sensor deployed by the science team and other standard shipboard sensing equipment to compensate for information that would have been difficult (or impossible) to collect with AUV *Sentry* otherwise. Without access to these external sensors, additional burdens would need to be placed on the environmental model and inference methods used for decision-making.

7.4 Inferring \mathbf{x}_p and \mathbf{x}_c

We used an MCMC methodology for estimating the initial conditions and model parameters, \mathbf{x}_p for a plume analytical model from observations. The use of this method allowed us to leverage the analytical model (the simulator) directly at the prediction and updating steps of PHUMES and lent considerable structure to the learning problem. On the other hand, we used a standard GP model to represent \mathbf{x}_c . In this case, there was no prior for how tides or other features may drive crossflow heading and velocity, but the availability of direct measurements (even at a single point) made training such a model straightforward. This perhaps highlights the importance the observation model (and task definition) has in selecting a useful model to represent belief over spatiotemporal environments. By decomposing \mathbf{x}_p and \mathbf{x}_c in the way we did, we were able to effectively apply a strong inductive bias to the learning problem that was most challenging for our available observations (determining the location of future plume waters).

In other formulations, \mathbf{x}_p and \mathbf{x}_c could have been “combined” and collectively represent a latent feature space; in such, the dual MCMC-GP methodology we used could be replaced with a generalized reinforcement learning or active learning framework. While such a method might be impractical for the small number of deployments possible while in the field, the use of sophisticated simulations of plume dynamics (e.g., [Xu and Di Iorio, 2012]) and robot physics in water could be effective in a pre-deployment training step and is worth considering in future work. One of the drawbacks of learned representations, however, is interpretability. \mathbf{x}_p as defined in this work directly corresponded to a set of physically-meaningful quantities that were understandable by the science party (who could then assess how “reasonable” any inferred value was). Moving forward, as more sophisticated models are necessary for challenging tasks in spatiotemporal environments, it may instead be beneficial to simultaneously learn both physically-meaningful quantities, and a latent space (perhaps relevant for a particular task). In scientific machine learning, these types of

architectures (e.g., [Raissi et al., 2019, Lu et al., 2020]) have already been proposed for fully-observable (or low-dimensional) settings, and may inspire methods adaptable for robotic science expeditions.

7.5 Embedding Autonomy Teams into a Science Party

As the desire for and use of robots for scientific expeditions increases, so too will the need for robust, autonomous systems. The state-of-the-art robotic fleet used in ocean sciences today represents well over a decade of effort put into creating physical embodiments that can successfully exist, navigate, and sample extreme environments. These robots perform critical mapping and surveying tasks, but are not yet leveraged to their full potential by science teams, in part due to the limits of their autonomous capabilities and the complexity of the tasks scientists want to complete. In brief, there is a need for autonomy engineers in science to co-develop *useful* models for decision-making (which may or may not align with useful models for science) and re-define science questions into actionable optimization problems. Expeditionary science challenges an autonomy engineer to develop both generalized/transferable skills for a robot between deployments or expeditions, in addition to purpose-built tools for niche phenomenon or queries. Attention to these purpose-built tools in robotics research is a frontier that this formulation of PHORTEX and PHUMES attempts to examine.

8 Future Work

There is a significant desire for embodied intelligence and assistive decision-making infrastructure for environmental exploration and expeditionary science. PHORTEX fundamentally relies on human expertise to inform the scientific models used within PHUMES, generate useful reward functions, set trajectory primitives, and operationally get deployed on a robot while in the field. Relieving the burden on these human agents—whether by creating aggregated data products or proposing multiple field missions with explanations—could lead to significant gains in the short-term for expeditionary science tasks while robot technology matures. For instance, on the research cruise in this study, we created science-data displays for AUV *Sentry* that displayed real-time science data reported at 0.002 Hz over acoustic modem. While a significantly limited subset of the data, this real-time reporting was sufficient for science experts to identify trends in robot performance with respect to the charting task. The capability of viewing real-time data, which to many academic and industrial roboticists may seem obvious or straightforward, is not yet pervasive or standard in the sciences or on state-of-the-art vessels and autonomous platforms. Research efforts on improving data infrastructure, data visualization, real-time signal processing, human decision-making, and supervised autonomy promise to be extremely impactful to the expeditionary sciences.

PHORTEX is an autonomy stack that has been demonstrated at-scale for a deployment-by-deployment mission to chart deep sea hydrothermal plumes, and showed quantitative gains over typical exploration strategies while also meshing into the operational ecosystem of a ship at sea. Future work specifically on developing autonomous systems for expeditionary science will push aspects of PHORTEX further, particularly focusing on adding sophistication to PHUMES spatiotemporal modeling from partial observations, increasing underway autonomy capabilities, and demonstrating improved scientific outcomes with this infrastructure. Several general open challenges in representation learning and decision-making for scientific expeditions of interest are:

- **Developing heterogeneous observation models:** Optimizing sample collection to address scientific hypotheses requires fusing different sensing modalities together and implementing complex observational models that link domain knowledge about sensor data to the state of a scientific phenomenon. Challenges include embedding expert knowledge into fused observational models, modeling sensor importance to a particular task, and reasoning across different sensors with distinct spatial and temporal resolutions (e.g., [Sarkar et al., 2014]).
- **Modeling aleatoric uncertainty:** There is a unique opportunity to compute proxies for aleatoric uncertainty, which are well-described in spatiotemporal environments with measures of chaotic motion (e.g., Lyapunov exponents) inferable from data [Blanchard and Sapsis, 2019]. The implication that aleatoric uncertainty can

be estimated has yet to be utilized to, e.g., assess the attainable resolution of a learned model or set planning horizons.

- **Leveraging scientific knowledge as inductive bias:** For data-driven discovery of spatiotemporal dynamics, improving sample efficiency by leveraging opportunities to inject scientific knowledge to alleviate the learning burden is an open problem. While canonical numerical models of spatiotemporal phenomena are too computationally expensive to directly incorporate into e.g., GP kernels, the physical principles that underlie these models can be more easily summarized via analytical models or learned surrogates; the field of scientific machine learning is ripe for adaptation in robotic IPP.
- **Rollout-based planning with expensive belief models:** State-of-the-art planners for POMDP problems often make use of rollout-based planning in tree search frameworks; continuous search variables are handled using strategies such as progressive widening or scenario sampling [Sunberg and Kochenderfer, 2018]. These planners require extensive online simulations for each rollout performed. Forward-simulating the dynamics and observational models for complex, spatiotemporal phenomena can be computationally intensive, which limits the feasible planning horizon in online decision-making. Planners that selectively or adaptively perform expensive rollouts, automatically adjust the planning horizon based on the dynamics of the environmental system, or make use of continuous, offline planners are necessary.
- **Abstractions for planning:** Instead of planning over a set of low-level, continuous control actions, planners could make use of high-level, abstract actions. These planning abstractions may come from human scientists or could be learned directly using recent developments in reinforcement learning and macro-action discovery [Flaspohler et al., 2020].
- **Robust planning under model mismatch and uncertainty:** Scientific models, whether data-driven or based on physical principles, are always imperfect representations of a robot’s environment. Model mismatch or uncertainty in key model parameters leads to discrepancies between the environmental predictions that a robot uses during planning and its real-time observations. Formal guarantees or well-characterized heuristic performance of planners under model mismatch is desired.
- **Interpretable and operational decision-making:** Decision-making algorithms must interface with and are constrained by a variety of stakeholders, including scientists, robot operators, and engineers. This requires developing flexible planners that can understand and account for these complex constraints. Additionally, stakeholders are often concerned with robot safety and data quality. Producing plans that are interpretable for scientific and operational stakeholders is key for building trust and confidence in scientific autonomy.

9 Conclusion

In this paper, we presented PHORTEX: **P**Hysically-informed **O**perational **R**obotic **T**rajectories for **E**Xpeditions, composed of a probabilistic model PHUMES that embedded an analytical science simulator to enable prediction of complex spatiotemporal dynamics and a trajectory optimizer which chained together operationally-constrained trajectory primitives into long-horizon deployments. The sequential decision-making loop (model update, trajectory design, trajectory execution) occurred in a deployment-by-deployment autonomy framework, which is well-suited to modern field operations and platforms.

We formulated PHORTEX for a specific instance of science expedition and platform: deep sea hydrothermal plume charting with AUV *Sentry*. Plume-charting asks a robot to map a spatiotemporally evolving plume structure, and using *Sentry* requires performing this task without underway adaptive capabilities and interpreting a complex, heterogeneous sensor suite. To this end, we formulated a task-relevant pseudo-sensor which processed *Sentry* data into a useful measurement of “plume occupancy” for *Sentry* which was used to update a formulation of PHUMES which embedded a plume-physics simulator and could additionally leverage external data sources to create forecasts of temporally discrete snapshots of 3D plume volumes. The trajectory optimizer used lawnmower primitives, as required by the *Sentry* team, to create long multi-hour trajectories which attempted to maximize the total number of plume detections that could be collected in the deployment window with the behavior constraint in place. These trajectories were then

validated using *Sentry* safety checks and deployed. Four deployments were conducted during a research cruise in November 2021, two of which were partially or completely planned using PHORTEX. We showed that in this setting, PHORTEX collected at least as many samples as human-designed surveys and showed improved spatial and temporal utilization for any given deployment.

We further validated PHORTEX in simulation, showing that...[TODO: simulation results pithy statement].

The modular PHORTEX framework can be easily adapted to other domain-specific tasks. The binary pseudo-sensor can be replaced with any discrete or continuous observation model appropriate for a particular platform or task; the scientific model leveraged within PHUMES could be trivially swapped for any other ODE or highly simplified PDE system (well-suited for e.g., ecological/population studies, fluid or thermal environments); and the reward function and trajectory optimization scheme can be modified based on the operational constraints of a target platform. The contribution of this work is to demonstrate the utility of incorporating domain-specific knowledge into autonomy frameworks for science, provide an example of how scientific knowledge and operational constraints can be formulated into a sophisticated (and deployable) autonomy schema, and introduce expeditionary science as a unique class of sequential decision-making problem.

Future work by this team will be specifically focused on enhancing representations of spatiotemporal distributions learned from sparse, partial observations using embedded scientific knowledge, developing interpretable and scalable inference schemes for decision-making by robotic and human agents, and developing more future-forward solutions for geochemical monitoring in oceanic environments with state-of-the-art robotic technologies actively used by science teams. Effective and intelligent expeditionary science and environmental exploration is a pressing societal challenge, and algorithmic development in service of expeditionary science presents many compelling technical opportunities in representation learning and decision-making for both deployment-by-deployment and underway autonomous systems.

Acknowledgments

Funding sources were [TODO: BLAH]. Many thanks to the Captain and crew of R/V Revelle, Sentry team engineers, and Jason team engineers who make expeditionary science possible, particularly S. Kelley, Z. Berkowitz, S. Suman, A. Sutherland, J. Fujii, J. Garcia. for their extensive help before and during sea trials with AUV Sentry. Additional thanks to S. Wankel, M. Jakuba, C. German, J. Kapit, W. Pardis, B. Colson, S. Youngs, X. Zhang, G. Xu, T. Barreyre, D. Martello, C. Cenedese, and D. Fornari for their support (engineering and professional), insights, and conversations.

References

- Agrawal, R. (1995). Sample mean based index policies by $\mathcal{O}(\log n)$ regret for the multi-armed bandit problem. *Adv. Appl. Probab.*, 27(4):1054–1078.
- Arora, A., Furlong, P. M., Fitch, R., Sukkarieh, S., and Fong, T. (2017). Multi-modal active perception for information gathering in science missions. In *Proc. Int. Symp. Auton. Robots*, pages 1–27.
- Auer, P. (2002). Using confidence bounds for exploitation-exploration trade-offs. *J. Mach. Learn. Research*, 3(Nov):397–422.
- Beaulieu, S. E., Baker, E. T., and German, C. R. (2015). Where are the undiscovered hydrothermal vents on oceanic spreading ridges? *Deep Sea Research Part II: Topical Studies in Oceanography*, 121:202–212.
- Binney, J. and Sukhatme, G. S. (2012). Branch and bound for informative path planning. In *Proc. IEEE Int. Conf. Robot. Autom.*, pages 2147–2154.
- Blanchard, A. and Sapsis, T. P. (2019). Analytical description of optimally time-dependent modes for reduced-order modeling of transient instabilities. *SIAM Journal on Applied Dynamical Systems*, 18(2):1143–1162.
- Branch, A., McMahon, J., Xu, G., Jakuba, M. V., German, C. R., Chien, S., Kinsey, J. C., Bowen, A. D., Hand, K. P., and Seewald, J. S. (2020). Demonstration of autonomous nested search for local maxima using an unmanned

- underwater vehicle. In *2020 IEEE International Conference on Robotics and Automation (ICRA)*, pages 1888–1895. IEEE.
- Browne, C. B., Powley, E., Whitehouse, D., Lucas, S. M., Cowling, P. I., Rohlfshagen, P., Tavener, S., Perez, D., Samothrakis, S., and Colton, S. (2012). A survey of Monte Carlo tree search methods. *IEEE Trans. Comput. Intell. AI Games*, 4(1):1–43.
- Camilli, R., Reddy, C. M., Yoerger, D. R., Van Mooy, B. A., Jakuba, M. V., Kinsey, J. C., McIntyre, C. P., Sylva, S. P., and Maloney, J. V. (2010). Tracking hydrocarbon plume transport and biodegradation at deepwater horizon. *Science*, 330(6001):201–204.
- Chen, W., Kharden, R., and Liu, L. (2022). Ak: Attentive kernel for information gathering. *arXiv preprint arXiv:2205.06426*.
- Chen, X.-x. and Huang, J. (2019). Odor source localization algorithms on mobile robots: A review and future outlook. *Robotics and Autonomous Systems*, 112:123–136.
- Chevaldonné, P., Desbruyères, D., and Le Haître, M. (1991). Time-series of temperature from three deep-sea hydrothermal vent sites. *Deep Sea Research Part A. Oceanographic Research Papers*, 38(11):1417–1430.
- Conn, A. R., Gould, N. I., and Toint, P. L. (2000). *Trust region methods*. SIAM.
- Corliss, J. B., Dymond, J., Gordon, L. I., Edmond, J. M., von Herzen, R. P., Ballard, R. D., Green, K., Williams, D., Bainbridge, A., Crane, K., et al. (1979). Submarine thermal springs on the galapagos rift. *Science*, 203(4385):1073–1083.
- Edwards, P. N. (2001). *Representing the global atmosphere: Computer models, data, and knowledge about climate change*, volume 1. MIT Press Cambridge, MA.
- Ferri, G., Jakuba, M. V., and Yoerger, D. R. (2010). A novel trigger-based method for hydrothermal vents prospecting using an autonomous underwater robot. *Autonomous Robots*, 29(1):67–83.
- Flaspholer, G., Preston, V., Michel, A. P., Girdhar, Y., and Roy, N. (2019). Information-guided robotic maximum seek-and-sample in partially observable continuous environments. *IEEE Robotics and Automation Letters*, pages 3782–3789.
- Flaspholer, G., Roy, N. A., and Fisher III, J. W. (2020). Belief-dependent macro-action discovery in POMDPs using the value of information. *Advances in Neural Information Processing Systems*, 33:11108–11118.
- Garg, S., Singh, A., and Ramos, F. (2012). Learning non-stationary space-time models for environmental monitoring. In *Twenty-Sixth AAAI Conference on Artificial Intelligence*.
- Geilert, S., Hensen, C., Schmidt, M., Liebetrau, V., Scholz, F., Doll, M., Deng, L., Fiskal, A., Lever, M. A., Su, C.-C., et al. (2018). On the formation of hydrothermal vents and cold seeps in the Guaymas Basin, Gulf of California. *Biogeosciences*, 15(18):5715–5731.
- Green, A., Singhal, R., and Venkateswar, R. (1980). Analytic extensions of the gaussian plume model. *Journal of the Air Pollution Control Association*, 30(7):773–776.
- Green, P. J. (1995). Reversible jump Markov chain Monte Carlo computation and Bayesian model determination. *Biometrika*, 82(4):711–732.
- Guestrin, C., Krause, A., and Singh, A. P. (2005). Near-optimal sensor placements in Gaussian processes. In *Proc. 22nd Int. Conf. Mach. Learn.*, pages 265–272. ACM.
- Hennig, P. and Schuler, C. J. (2012). Entropy search for information-efficient global optimization. *J. Mach. Learn. Res.*, 13(Jun):1809–1837.
- Hernández-Lobato, J. M., Hoffman, M. W., and Ghahramani, Z. (2014). Predictive entropy search for efficient global optimization of black-box functions. In *Proc. 27th Int. Conf. Neural Inf. Process. Syst.*, pages 918–926.

- Hitz, G., Galceran, E., Garneau, M.-È., Pomerleau, F., and Siegwart, R. (2017). Adaptive continuous-space informative path planning for online environmental monitoring. *J. Field Robot.*, 34(8):1427–1449.
- Jakuba, M. V. (2007). *Stochastic mapping for chemical plume source localization with application to autonomous hydrothermal vent discovery*. PhD thesis, Massachusetts Institute of Technology.
- Jannasch, H. W. and Mottl, M. J. (1985). Geomicrobiology of deep-sea hydrothermal vents. *Science*, 229(4715):717–725.
- Jawaid, S. T. and Smith, S. L. (2015). Informative path planning as a maximum traveling salesman problem with submodular rewards. *Discr. Appl. Math.*, 186:112–127.
- Jones, D. R., Schonlau, M., and Welch, W. J. (1998). Efficient global optimization of expensive black-box functions. *J. Global Optim.*, 13(4):455–492.
- Kaiser, C. L., Yoerger, D. R., Kinsey, J. C., Kelley, S., Billings, A., Fujii, J., Suman, S., Jakuba, M., Berkowitz, Z., German, C. R., et al. (2016). The design and 200 day per year operation of the autonomous underwater vehicle sentry. In *2016 IEEE/OES Autonomous Underwater Vehicles (AUV)*, pages 251–260. IEEE.
- Kim, J., Son, S.-K., Kim, D., Pak, S.-J., Yu, O. H., Walker, S. L., Oh, J., Choi, S. K., Ra, K., Ko, Y., et al. (2020). Discovery of active hydrothermal vent fields along the central indian ridge, 8–12 s. *Geochemistry, Geophysics, Geosystems*, 21(8):e2020GC009058.
- Krause, A., Singh, A., and Guestrin, C. (2008a). Near-optimal sensor placements in Gaussian processes: Theory, efficient algorithms and empirical studies. *Journal of Machine Learning Research*, 9(2).
- Krause, A., Singh, A., and Guestrin, C. (2008b). Near-Optimal Sensor Placements in Gaussian Processes: Theory, Efficient Algorithms and Empirical Studies. *J. Mach. Learn. Res.*, 9:235–284.
- Kushner, H. J. (1964). A new method of locating the maximum point of an arbitrary multipeak curve in the presence of noise. *J. Basic Eng.*, 86(1):97–106.
- Lavelle, J., Di Iorio, D., and Rona, P. (2013). A turbulent convection model with an observational context for a deep-sea hydrothermal plume in a time-variable cross flow. *Journal of Geophysical Research: Oceans*, 118(11):6145–6160.
- Li, S., Guo, Y., and Bingham, B. (2014). Multi-robot cooperative control for monitoring and tracking dynamic plumes. In *2014 IEEE International Conference on Robotics and Automation (ICRA)*, pages 67–73. IEEE.
- Lim, Z. W., Hsu, D., and Lee, W. S. (2016). Adaptive informative path planning in metric spaces. *Int. J. Robot. Res.*, 35(5):585–598.
- Lu, P. Y., Kim, S., and Soljacić, M. (2020). Extracting interpretable physical parameters from spatiotemporal systems using unsupervised learning. *Physical Review X*, 10(3):031056.
- Ludwig, F., Gasiorek, L., and Ruff, R. (1977). Simplification of a gaussian puff model for real-time minicomputer use. *Atmospheric Environment* (1967), 11(5):431–436.
- Luo, W. and Sycara, K. (2018). Adaptive sampling and online learning in multi-robot sensor coverage with mixture of gaussian processes. In *IEEE Int. Conf. Robot. Autom.*, pages 6359–6364. IEEE.
- Ma, K.-C., Liu, L., and Sukhatme, G. S. (2017). Informative planning and online learning with sparse gaussian processes. In *2017 IEEE International Conference on Robotics and Automation (ICRA)*, pages 4292–4298. IEEE.
- MacKay, D. J. (1998). Introduction to Monte Carlo methods. In *Learning in graphical models*, pages 175–204. Springer.
- Marchant, R., Ramos, F., and Sanner, S. (2014). Sequential Bayesian optimisation for spatial-temporal monitoring. In *Proc. 13th Conf. Uncertainty Artif. Intell.*, pages 553–562.

- Martin, W., Baross, J., Kelley, D., and Russell, M. J. (2008). Hydrothermal vents and the origin of life. *Nature Reviews Microbiology*, 6(11):805–814.
- Mason, J. C., Branch, A., Xu, G., Jakuba, M. V., German, C. R., Chien, S., Bowen, A. D., Hand, K. P., and Seewald, J. S. (2020). Evaluation of auv search strategies for the localization of hydrothermal venting.
- Mcgill, K. and Taylor, S. (2011). Robot algorithms for localization of multiple emission sources. *ACM Computing Surveys (CSUR)*, 43(3):1–25.
- Metropolis, N., Rosenbluth, A. W., Rosenbluth, M. N., Teller, A. H., and Teller, E. (1953). Equation of state calculations by fast computing machines. *The journal of chemical physics*, 21(6):1087–1092.
- Morse, T. M., Lockery, S. R., and Ferrée, T. C. (1998). Robust spatial navigation in a robot inspired by chemotaxis in *caenorhabditis elegans*. *Adaptive Behavior*, 6(3-4):393–410.
- Morton, B., Taylor, G. I., and Turner, J. S. (1956). Turbulent gravitational convection from maintained and instantaneous sources. *Proceedings of the Royal Society of London. Series A. Mathematical and Physical Sciences*, pages 1–23.
- Nakamura, K., Toki, T., Mochizuki, N., Asada, M., Ishibashi, J.-i., Nogi, Y., Yoshikawa, S., Miyazaki, J.-i., and Okino, K. (2013). Discovery of a new hydrothermal vent based on an underwater, high-resolution geophysical survey. *Deep Sea Research Part I: Oceanographic Research Papers*, 74:1–10.
- Neal, R. M. et al. (2011). MCMC using Hamiltonian dynamics. *Handbook of Markov chain Monte Carlo*, pages 113–162.
- Nemhauser, G. L., Wolsey, L. A., and Fisher, M. L. (1978). An analysis of approximations for maximizing submodular set functions—i. *Math. Program.*, 14(1):265–294.
- Ouyang, R., Low, K. H., Chen, J., and Jaillet, P. (2014). Multi-robot active sensing of non-stationary gaussian process-based environmental phenomena. In *Proc. Int. Conf. Auton. Agents. Multiagent Sys.*, pages 573–580. Int. Foundation Auton. Agents Multiagent Sys.
- Paduan, J. B., Zierenberg, R. A., Clague, D. A., Spelz, R. M., Caress, D. W., Troni, G., Thomas, H., Glessner, J., Lilley, M. D., Lorenson, T., et al. (2018). Discovery of hydrothermal vent fields on alarcón rise and in southern pescadero basin, gulf of california. *Geochemistry, Geophysics, Geosystems*, 19(12):4788–4819.
- Peng, L., Lipinski, D., and Mohseni, K. (2014). Dynamic data driven application system for plume estimation using uavs. *Journal of Intelligent & Robotic Systems*, 74(1):421–436.
- Raiissi, M., Perdikaris, P., and Karniadakis, G. E. (2018). Numerical gaussian processes for time-dependent and nonlinear partial differential equations. *SIAM Journal on Scientific Computing*, 40(1):A172–A198.
- Raiissi, M., Perdikaris, P., and Karniadakis, G. E. (2019). Physics-informed neural networks: A deep learning framework for solving forward and inverse problems involving nonlinear partial differential equations. *Journal of Computational Physics*, 378:686–707.
- Reddy, G., Murthy, V. N., and Vergassola, M. (2022). Olfactory sensing and navigation in turbulent environments. *Annual Review of Condensed Matter Physics*, 13.
- Salam, T. and Hsieh, M. A. (2019). Adaptive sampling and reduced-order modeling of dynamic processes by robot teams. *IEEE Robotics and Automation Letters*, 4(2):477–484.
- Sarkar, S., Sarkar, S., Virani, N., Ray, A., and Yasar, M. (2014). Sensor fusion for fault detection and classification in distributed physical processes. *Frontiers in Robotics and AI*, 1:16.
- Särkkä, S. (2013). *Bayesian filtering and smoothing*. Number 3. Cambridge university press.
- Silver, D. and Veness, J. (2010). Monte-Carlo planning in large POMDPs. In *Proc. Adv. Neural Inf. Process. Syst.*, pages 2164–2172.

- Singh, A., Krause, A., and Kaiser, W. J. (2009). Nonmyopic adaptive informative path planning for multiple robots. In *Proc. 21st Int. Joint Conf. Artif. Intell.*, pages 1843–1850.
- Singh, A., Ramos, F., Whyte, H. D., and Kaiser, W. J. (2010). Modeling and decision making in spatio-temporal processes for environmental surveillance. In *2010 IEEE International Conference on Robotics and Automation*, pages 5490–5497. IEEE.
- Snoek, J., Larochelle, H., and Adams, R. P. (2012). Practical Bayesian optimization of machine learning algorithms. In *Proc. Adv. Neural Info. Process. Syst.*, pages 2951–2959.
- Soule, S. A., Seewald, J., Wankel, S. D., Michel, A., Beinart, R., Briones, E. E., Dominguez, E. M., Girguis, P., Coleman, D., Raineault, N. A., et al. (2018). Exploration of the Northern Guaymas Basin. *Oceanography*, 31(1):39–41.
- Speer, K. G. and Rona, P. A. (1989). A model of an atlantic and pacific hydrothermal plume. *Journal of Geophysical Research: Oceans*, 94(C5):6213–6220.
- Srinivas, N., Krause, A., Kakade, S. M., and Seeger, M. W. (2012). Information-Theoretic Regret Bounds for Gaussian Process Optimization in the Bandit Setting. *IEEE Trans. Inf. Theory*, 58:3250–3265.
- Sunberg, Z. N. and Kochenderfer, M. J. (2018). Online algorithms for POMDPs with continuous state, action, and observation spaces. In *Proc. 24th Int. Conf. Automated Plan. Schedul.*
- Tohidi, A. and Kaye, N. B. (2016). Highly buoyant bent-over plumes in a boundary layer. *Atmospheric Environment*, 131:97–114.
- Vergassola, M., Villermaux, E., and Shraiman, B. I. (2007). ‘infotaxis’ as a strategy for searching without gradients. *Nature*, 445(7126):406–409.
- Wan, Z. Y. and Sapsis, T. P. (2017). Reduced-space gaussian process regression for data-driven probabilistic forecast of chaotic dynamical systems. *Physica D: Nonlinear Phenomena*, 345:40–55.
- Wang, L., Pang, S., and Xu, G. (2020). 3-dimensional hydrothermal vent localization based on chemical plume tracing. In *Global Oceans 2020: Singapore–US Gulf Coast*, pages 1–7. IEEE.
- Welch, G., Bishop, G., et al. (1995). An introduction to the kalman filter.
- Wilson, A. G., Hu, Z., Salakhutdinov, R., and Xing, E. P. (2016). Deep kernel learning. In *Artificial Intelligence and Statistics*, pages 370–378.
- Xu, G. and Di Iorio, D. (2012). Deep sea hydrothermal plumes and their interaction with oscillatory flows. *Geochemistry, Geophysics, Geosystems*, 13(9).